A MULTIOBJECTIVE OPTIMIZATION TOOLBOX DEVELOPMENT FOR PARAMETER IDENTIFICATION OF ELASTOMERS

A THESIS SUBMITTED TO
THE GRADUATE SCHOOL OF NATURAL AND APPLIED SCIENCES
OF
MIDDLE EAST TECHNICAL UNIVERSITY

BY

TANYEL TEKİN

IN PARTIAL FULFILLMENT OF THE REQUIREMENTS
FOR
THE DEGREE OF MASTER OF SCIENCE
IN
MECHANICAL ENGINEERING

JANUARY 2018

Approval of the thesis:

A MULTIOBJECTIVE OPTIMIZATION TOOLBOX DEVELOPMENT FOR PARAMETER IDENTIFICATION OF ELASTOMERS

submitted by **TANYEL TEKİN** in partial fulfillment of the requirements for the degree of **Master of Science in Mechanical Engineering Department, Middle East Technical University** by,

Prof. Dr. Gülbin Dural Ünver   _____
Dean, Graduate School of **Natural and Applied Sciences**

Prof. Dr. M. A. Sahir Arıkan   _____
Head of Department, **Mechanical Engineering**

Asst. Prof. Dr. Hüsnü Dal   _____
Supervisor, **Mechanical Engineering Dept., METU**

Examining Committee Members:

Prof. Dr. Süha Oral   _____
Mechanical Engineering Dept., METU

Asst. Prof. Dr. Hüsnü Dal   _____
Mechanical Engineering Dept., METU

Prof. Dr. Suat Kadıoğlu   _____
Mechanical Engineering Dept., METU

Assoc. Prof. Dr. Demirkan Çöker   _____
Mechanical Engineering Dept., METU

Asst. Prof. Dr. Celal Evci   _____
Mechanical Engineering Dept., Atılım University

Date: 22/01/2018

I hereby declare that all information in this document has been obtained and presented in accordance with academic rules and ethical conduct. I also declare that, as required by these rules and conduct, I have fully cited and referenced all material and results that are not original to this work.

Name, Last Name: TANYEL TEKİN

Signature   :

ABSTRACT

A MULTIOBJECTIVE OPTIMIZATION TOOLBOX DEVELOPMENT FOR PARAMETER IDENTIFICATION OF ELASTOMERS

Tekin, Tanyel

M.S., Department of Mechanical Engineering

Supervisor: Asst. Prof. Dr. Hüsnü Dal

January 2018, 80 pages

Rubber materials are widely used in industry because of their hyperelastic behaviors. Rubber materials show a highly nonlinear behavior due to hyperelastic deformability. Thus, small strain theory can not be applied to rubber materials. Various hyperelastic models are proposed by different researchers by deriving stress-stretch relations. Those relations differ in various test conditions including uniaxial, equibiaxial, pure shear and biaxial deformation modes. In this thesis, ten hyperelastic models including phenomenological and micro-mechanical models are examined. Stress definitions are obtained. Then, their efficiencies are compared by using related experimental data sets. Finally, a multiobjective optimization toolbox is developed in MATLAB GUI.

Treloar data are used for parameter identification of rubber models in uniaxial, equibiaxial and pure shear cases after stress definitions are obtained for related model. Deformation gradient, right and left Cauchy-Green tensor and Kirchhoff stress differ according to each case. The Kirchhoff stresses are also decomposed

into volumetric and isochoric parts. The other stresses are used in continuum mechanics are the first and second Piola-Kirchhoff stresses and Cauchy stress. The data which are used for validation of biaxial case are Kawabata data in this study. In biaxial case, the material is stretched from two orthogonal directions with different ratios. This leads to different stretches in two orthogonal directions. If those stretches are same, the case becomes equibiaxial case. In biaxial case, same tensors are obtained like other cases. In Kawabata data, there are data for stress-stretch in two directions. In present research, stress data of one of these directions are used for parameter identification procedure.

ÖZ

ELASTOMERLERİN PARAMETRELERİNİN TANIMLANMASI İÇİN ÇOK AMAÇLI BİR ENİYİLEME PROGRAMI GELİŞTİRİLMESİ

Tekin, Tanyel

Yüksek Lisans, Makine Mühendisliği Bölümü

Tez Yöneticisi: Y. Doç. Dr. Hüsnü Dal

Ocak 2018, 80 sayfa

Kauçuk malzemelerin hiperelastik davranışları sebebiyle endüstride geniş kullanım alanları mevcuttur. Kauçuk malzemeler uğradıkları hiperelastik deformasyon sebebiyle yüksek derecede doğrusal olmayan davranış gösterirler. Bu sebeple küçük gerinim teorisi kauçuk malzemeler için uygulanabilir değildir. Farklı araştırmacılar tarafından çeşitli hiperelastik modeller gerilim-gerinim ilişkileri türetilerek sunulmuştur. Bu ilişkilendirmeler tek eksenli, eşikieksenli, saf kayma ve iki eksenli olmak üzere çeşitli test koşulları altında değişmektedir. Bu tezde fenomenolojik ve mikro-mekanik hiperelastik modelleri içeren toplam on adet model incelenmiştir. Gerilme tanımlamaları elde edilmiştir. Daha sonra bu modellerin etkinlikleri ilgili veri setleri kullanılarak karşılaştırılmıştır. Son olarak çok amaçlı bir eniyileme programı MATLAB GUI'de geliştirilmiştir.

Treloar verisi tek eksenli, eşikieksenli ve saf kayma test koşullarında kauçuk modellerindeki gerilme ifadeleri bulunduktan sonra ilgili modelin parametrelerinin tanımlanması için kullanılmaktadır. Deformasyon değişimi, sağ ve sol Cauchy-

Green tensörleri ve Kirchhoff gerilme ifadeleri her test koşulunda değişmektedir. Kirchhoff gerilmesi volümetrik ve izokorik olarak iki kısma ayrılmaktadır. Birinci ve ikinci Piola-Kirchhoff gerilmeleri ve Cauchy gerilmesi de sürekli ortamlar mekaniğinde kullanılan diğer gerilmelerdir.

İki eksenli test koşulu doğrulanması için kullanılan veri ise Kawabata verisidir. İki eksenli test koşulunda malzeme ortogonal iki eksenden farklı oranlarda uzatılmaktadır. Bu sebeple bu iki ortogonal eksende farklı uzamalar gerçekleşmektedir. Eğer bu eksenlerdeki uzama miktarları aynı olursa, test koşulu eşikieksenli durumu olur. Diğer test koşullarında olduğu gibi ilgili tensörler iki eksenli durum için de elde edilir. Kawabata verisinde iki farklı yön için iki farklı gerilme-uzama verisi bulunmaktadır. Bu çalışmada parameter tanımlanması prosedürü için bu yönlerden birindeki gerilme verileri kullanılmaktadır.

Anahtar Kelimeler: Hiperelastisite, Kauçuk Malzeme, Parametre Tanımlanması, Kauçuk Modelleri, Fenomenolojik Modeller, Mikro-mekanik Modeller, MATLAB GUI

To My Wife and Family

ACKNOWLEDGMENTS

TABLE OF CONTENTS

LIST OF TABLES

TABLES

LIST OF FIGURES

FIGURES

LIST OF SYMBOLS

F	Deformation gradient
F̄	Modified deformation gradient
C	The right Cauchy-Green deformation tensor
C̄	Isochoric right Cauchy-Green deformation tensor
B	The left Cauchy-Green deformation tensor (finger tensor)
u	Displacement, m
x	Position of deformed vector, m
X	Position of undeformed vector, m
J	Jacobian determinant
W	Free energy function
δ	Kronecker delta
I	Identity tensor
$\hat{p}$	Hydrostatic pressure, MPa
m	Meter
v	Deformed volume, m^3
V	Undeformed volume, m^3
λ	Stretch

$\bar{\lambda}$	Modified stretch
n	Normal vector of deformed area
N	Normal vector of undeformed area
MPa	MegaPascal
P	First Piola-Kirchhoff stress tensor, MPa
σ	Cauchy Stress, MPa
S	Second Piola-Kirchhoff stress tensor, MPa
I	Strain invariant
τ	Kirchhoff Stress Tensor, MPa
τ̂	Isochoric Kirchhoff Stress Tensor, MPa
E	Modulus of elasticity, MPa
v	Poisson ratio
μ	Shear modulus, MPa
$\mathcal{L}$	Langevin function
t	Traction vector in deformed configuration, Pa
T	Traction vector in undeformed configuration, Pa
N	Newton
ΔF	Force element, N
ΔA	Area element, m^2

f	Force acting on the surface in the deformed configuration, N
Θ	Absolute temperature, K
k_b	Boltzmann's constant, Joule/K
K	Kelvin
GUI	Graphical User Interface

CHAPTER 1

INTRODUCTION

1.1. Motivation

Rubber materials are widely used in industry because of their hyperelastic behavior. They have a lot of applications especially in automotive industry. For instance, windshield wipers, transmission belts, washers, seals, gaskets and o-rings are made of rubber materials [1].

Solid materials are classified as metal, ceramic, polymers and composite materials. Polymeric materials have become significant materials due to their lightness and easy-machinability. Rubber materials are in polymeric material class.

The macromolecules which are connected to each other via cross-links or entanglements form the rubber materials. Thus, rubber materials exhibit very high extensions under certain forces. Moreover, they can return to nearly their first length when the forces are removed. This property is based on low cross-link density and nonuniform structure. Permanent deformation is prevented by cross-links in the rubber structure.

Rubber materials exhibit a highly nonlinear behavior because of hyperelastic deformability. Thus, they can not be evaluated by small strain theory. In small strain theory, deformed and undeformed configurations are nearly same. However, this may not be true for rubber materials. Those two configurations must be examined separately. Moreover, they have to be related with certain tensors including stress and strain tensors.

Free energy functions are used to have constitutive equations of rubber materials to obtain stress-stretch relations. Two approaches for the study of rubber elasticity are

put forward. First approach is to have a phenomenological formulation for free energy function. The other approach is to derive rubber properties from idealized rubber structure models [2]. These models are important because appropriate rubber material model and its parameters lead to have correct results in finite element simulations.

There are various hyperelastic constitutive rubber models and the problem is to use the best fitting material model with appropriate material parameters for related application. The nonlinear stretch-stress curves of rubber materials seem like 'S' letter. A rubber model should reproduce 'S' shaped response of rubbers, not to have problem with different deformation modes, have material parameters as few as possible, have a simple mathematical formulation as much as possible [3]. For this purpose, some studies have been conducted to identify material parameters of rubber models. Moreover, different experimental data like Treloar [4] and Kawabata [5] data are used to validate the results.

It must be noted that those classical hyperelastic models of rubbers are more applicable to cross-linked rubbers due to cross-links' providing the material elasticity property [6]. Also, those models are not used for mechanisms like material softening. The researchers should apply another approaches for these phenomena [7].

1.2. Objective

The objective of this thesis is to develop a multiobjective optimization toolbox for parameter identification of elastomers.

Ten hyperelastic rubber models involving phenomenological and micro-mechanical models are examined. Stress-stretch relations for those models are presented. A parameter identification algorithm is proposed. According to this algorithm, material parameters of ten hyperelastic rubber models are identified. Two material parameter sets are identified for each model. First material parameter set is used for

uniaxial, equibiaxial and pure shear cases for related model. Treloar data are used in this case for identification process. Second parameter set is used for biaxial case for related model. Kawabata data are used in this case for identification process. A multiobjective optimization toolbox is developed in MATLAB GUI to perform all those calculations faster and more easily. Furthermore, efficiency of rubber models are compared according to specified criteria.

1.3. Thesis Overview

Chapter 2 provides a detailed description of theoretical background for continuum mechanics preliminaries and literature studies are given in this chapter. Hyperelastic models' stress-stretch expression calculations are given in Chapter 3. Chapter 4 addresses the parameter identification algorithm and multiobjective toolbox development in MATLAB GUI. Chapter 5 shows the parameter identification results of hyperelastic models in uniaxial, equibiaxial, pure shear cases and biaxial case. Chapter 6 provides a summary of identification process results, results' comparison and conclusions.

CHAPTER 2

THEORETICAL BACKGROUND

2.1. Continuum Mechanics Preliminaries

2.1.1. Deformation Tensors

The terms of a strain energy function which is power series in the invariants of deformation tensors can describe elastic properties of a rubber material. For this purpose, the right and left Cauchy-Green deformation tensors, respectively $\mathbf{C}$ and $\mathbf{B}$ should be presented. Thus, invariants of deformation tensors can be found as

$$\mathbf{C} = \mathbf{F}^T\mathbf{F} \text{ and } \mathbf{B} = \mathbf{FF}^T. \tag{2.1}$$

Here, $\mathbf{F}$ is deformation gradient. The deformation gradient $\mathbf{F}$ is the measure of deformation in continuum mechanics. The deformation gradient is a tensor quantifying not only both 2D and 3D shape change but also whole material rotation. From Figure 2.1, deformation gradient mapping a line element from undeformed configuration to deformed configuration can be seen. The deformation gradient is calculated by performing derivation of the position of deformed $\mathbf{x}$ vector to the position of $\mathbf{X}$ undeformed reference vector as

$$F_{ij} = x_{i,j} = \frac{\partial x_i}{\partial X_j} = \begin{bmatrix} \dfrac{\partial x_1}{\partial X_1} & \dfrac{\partial x_1}{\partial X_2} & \dfrac{\partial x_1}{\partial X_3} \\ \dfrac{\partial x_2}{\partial X_1} & \dfrac{\partial x_2}{\partial X_2} & \dfrac{\partial x_2}{\partial X_3} \\ \dfrac{\partial x_3}{\partial X_1} & \dfrac{\partial x_3}{\partial X_2} & \dfrac{\partial x_3}{\partial X_3} \end{bmatrix}. \tag{2.2}$$
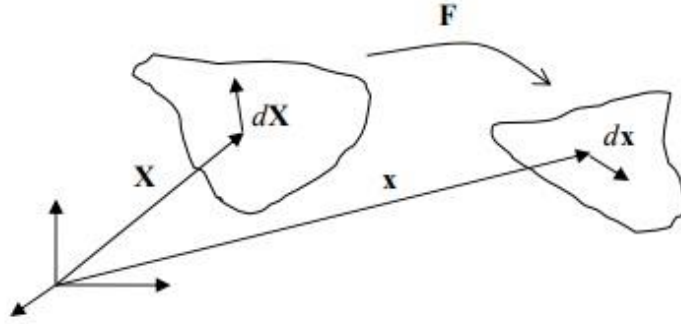
Figure 2.1: Deformation gradient mapping a line element from undeformed configuration to deformed configuration

Displacement **u** also can be calculated as

$$\mathbf{u} = \mathbf{x} - \mathbf{X}. \tag{2.3}$$

That means **x= u+X** and if we substitute equation (2.3) into equation (2.2), **F** can be calculated as

$$\mathbf{F} = \frac{\partial(\mathbf{X} + \mathbf{u})}{\partial \mathbf{X}} = \mathbf{I} + \frac{\partial \mathbf{u}}{\partial \mathbf{X}}. \tag{2.4}$$

In tensor notation, it can be written as

$$F_{ij} = \delta_{ij} + u_{i,j}. \tag{2.5}$$

Invariants of deformation tensors can be written as

$$I_1 = \text{tr}(\mathbf{C}) = \text{tr}(\mathbf{B}), \tag{2.6}$$

$$I_2 = \frac{1}{2}\left[\left(\text{tr}(\mathbf{C})\right)^2 - \text{tr}(\mathbf{C}\mathbf{C})\right] = \frac{1}{2}[(\text{tr}(\mathbf{B}))^2 - \text{tr}(\mathbf{B}\mathbf{B})], \tag{2.7}$$

$$\text{and } I_3 = \det(\mathbf{C}) = \det(\mathbf{B}) = J^2. \tag{2.8}$$

6

Here, J is a measure of change in volume. It is called as Jacobian determinant. J is found as

$$J(\mathbf{X}, t) = \det\mathbf{F} = \begin{vmatrix} \dfrac{\partial x_1}{\partial X_1} & \dfrac{\partial x_1}{\partial X_2} & \dfrac{\partial x_1}{\partial X_3} \\[8pt] \dfrac{\partial x_2}{\partial X_1} & \dfrac{\partial x_2}{\partial X_2} & \dfrac{\partial x_2}{\partial X_3} \\[8pt] \dfrac{\partial x_3}{\partial X_1} & \dfrac{\partial x_3}{\partial X_2} & \dfrac{\partial x_3}{\partial X_3} \end{vmatrix}. \tag{2.9}$$

Since J shows how deformation changes the volume of a material, it is called as volume ratio and volume change can be calculated as

$$dv = JdV. \tag{2.10}$$

Here, dV is undeformed (reference) volume element and dv is deformed (current) volume element. Since volumes must be positive and $\mathbf{F}$ has inverse, J must be bigger than 0 (zero). For incompressible case, volume change is 0 (zero). For this case, J must be 1 (one).

After invariants of deformation tensors are given, at this point stretch, λ , must be defined. The ratio of the length of a deformed line element to the same element's undeformed line element length is called as the stretch. Its calculation is given as

$$\lambda = \frac{|d\mathbf{x}|}{|d\mathbf{X}|}. \tag{2.11}$$

Here, eigenvalue decomposition of tensors $\mathbf{C}$ and $\mathbf{B}$ can be written as

$$\mathbf{B} = \sum_{A=1} \lambda_A^2\, \mathbf{n_A} \otimes \mathbf{n_A} \text{ and} \tag{2.12}$$

$$\mathbf{C} = \sum_{A=1} \lambda_A^2\, \mathbf{N_A} \otimes \mathbf{N_A}. \tag{2.13}$$

7

Here λ_A are principal stretches and $\mathbf{n}_A$, $\mathbf{N}_A$ are components of normal vectors of corresponding tensors. Principal stretches and invariants of deformation gradients have the relations as

$$I_1 = \text{tr}(\mathbf{B}) = \lambda_1^2 + \lambda_2^2 + \lambda_3^2 \,, \tag{2.14}$$

$$I_2 = \frac{1}{2}\left[I_1^{\,2} - \text{tr}(\mathbf{BB})\right] = \lambda_1^2\lambda_2^2 + \lambda_1^2\lambda_3^2 + \lambda_2^2\lambda_3^2 \text{ and} \tag{2.15}$$

$$I_3 = \det(\mathbf{B}) = \lambda_1^2\lambda_2^2\lambda_3^2. \tag{2.16}$$

If material is incompressible, it leads to the definition

$$I_3 = 1. \tag{2.17}$$

2.1.2.   Stress Tensors

When deformation gradient is presented in the previous part, deformed and undeformed configurations are shown in the Figure 2.1. If the deformations are small, there is not a prominent difference between deformed and undeformed configurations. Thus, Cauchy stress (true stress) can be used for describing the actions of surface forces for each configuration. The limiting value of the ratio of force over area is called as the traction vector and it is calculated as

$$\mathbf{t}^{(\mathbf{n})} = \lim_{\Delta A \to 0} \frac{\Delta F}{\Delta A}. \tag{2.18}$$

Cauchy stress can be calculated as

$$\mathbf{t} = \boldsymbol{\sigma}\mathbf{n} \text{ and} \tag{2.19}$$

in tensor notation, it can be written as

$$t_i = \sigma_{ij}n_j. \tag{2.20}$$

In full notation, traction vector components can be written as

$$t_1 = \sigma_{11}n_1 + \sigma_{12}n_2 + \sigma_{13}n_3 \,, \tag{2.21}$$

$$t_2 = \sigma_{21}n_1 + \sigma_{22}n_2 + \sigma_{23}n_3 \text{ and} \tag{2.22}$$

$$t_3 = \sigma_{31}n_1 + \sigma_{32}n_2 + \sigma_{33}n_3 . \tag{2.23}$$

Components of Cauchy stress distributed on a cubic element are shown in Figure 2.2.
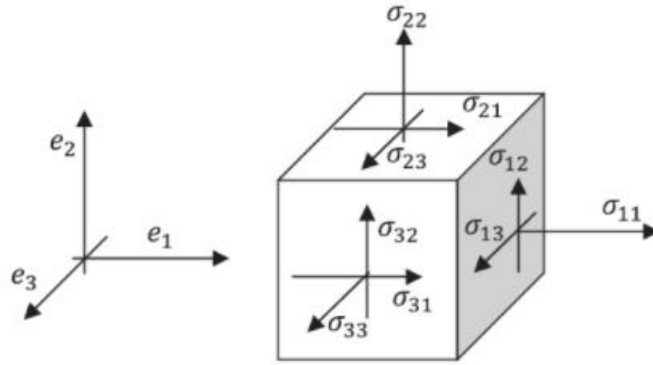
Figure 2.2: Components of Cauchy stress distributed on a cubic element

If the deformations are large, reference configuration must be defined. In this case, Cauchy stress will not be enough. There are also different ways of defining the action of surface forces.

The first Piola-Kirchhoff stress tensor, **P**, can be written as

$$d\mathbf{f} = \mathbf{P}\mathbf{N}dA. \tag{2.24}$$

Here, $d\mathbf{f}$ is the force acting on the surface element in the current configuration. dA is the area of the element. **N** is the unit normal. It should be noted that in reference configuration capital letters are used for notation whereas small letters are used in current configuration. It means that **n** will be used for unit normal in current configuration and $d\mathbf{a}$ will be used for area of the element in the current configuration. Traction vectors acting on the reference and current configurations can be seen in Figure 2.3.
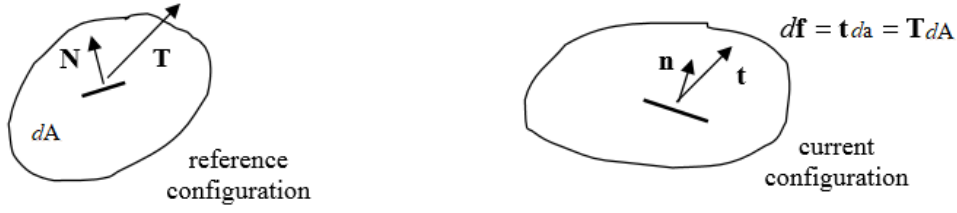
Figure 2.3: Traction vectors acting on the reference and current configurations

It can be seen from equation (2.24) that the first Piola-Kirchhoff stress tensor is a two-point tensor because the surface element in the reference configuration is related to the force acting on the current configuration by this stress tensor. The relation between Cauchy stress and the first Piola-Kirchhoff stress can be written as

$$\boldsymbol{\sigma}\mathbf{n}da = \mathbf{PN}dA. \tag{2.25}$$

In this point Piola transform can be used as

$$\mathbf{n}da = J\mathbf{F}^{-T}\mathbf{N}dA. \tag{2.26}$$

If we substitute Piola transform into equation (2.25), the first Piola-Kirchhoff stress becomes

$$\mathbf{P} = J\boldsymbol{\sigma}\mathbf{F}^{-T}. \tag{2.27}$$

The second Piola-Kirchhoff stress tensor, **S,** can be written as

$$\mathbf{S} = J\mathbf{F}^{-1}\boldsymbol{\sigma}\mathbf{F}^{-T}. \tag{2.28}$$

The second Piola-Kirchhoff stress tensor is a symmetric tensor. The first and second Piola-Kirchhoff stresses can be related as

$$\mathbf{P} = \mathbf{FS}. \tag{2.29}$$

Kirchhoff stress tensor, $\boldsymbol{\tau}$, is defined as

$$\boldsymbol{\tau} = J\boldsymbol{\sigma}. \tag{2.30}$$

Kirchhoff stress is the push forward of the second Piola-Kirchhoff stress tensor. It can be calculated as

$$\tau = \mathbf{F}\mathbf{S}\mathbf{F}^{\mathrm{T}}. \tag{2.31}$$

There are more stress definitions which are used in continuum mechanics but in this thesis, the stresses explained above are used. It must be noted that those stress measures are all equivalent in small strain theory. If the deformations are small, terms involving products of displacement gradients are neglected. Then, it is applicable for metals. However, rubber materials can not be evaluated with small strain theory due to hyperelastic deformation. This also leads rubber materials to have nonlinear behavior.

2.1.3.   Deformation Modes

As it was stated before, the design of metallic materials can be easily done since they have rather easier constitutive equations than rubber materials. Metallic materials, in elastic region, exhibit same behavior either in compression or in tension. In constitutive equations of metals, modulus of elasticity (E) and Poisson ratio (v) can be easily obtained by a simple uniaxial tension test. Thus, finite element analyses of metallic materials can be performed easily. However, this situation is completely different for rubber materials. Rubber materials have different chemical, mechanical and thermal properties than metals. Thus, obtaining constitutive equations of rubber materials are more difficult.

Constitutive equations of rubber materials can not be defined directly by stress-strain relations with required accuracy. Thus, free energy functions are used to have constitutive equations of rubber materials. Forming a free energy function is the initiating point of hyperelastic rubber modeling. Various researches proposed different free energy functions with different methods [1].

After free energy function is obtained, material parameters in those free energy functions must be identified with certain material tests. In these tests, nominal stress vs. nominal strain data are required. It should be noted that experiments are cost-intensive and time consuming. Thus, having a simpler free energy function with

11

minimized number of material parameters is desirable. More common tests which are performed for rubber materials are uniaxial tension, equibiaxial tension, pure shear and biaxial tension. Those deformation modes are used in this thesis.

Uniaxial tension is the more common and simpler deformation mode. Moreover, this experiment is commonly performed for rubber materials. The key point in this experiment is that the length of the specimen in the direction of stretching must be much longer than other dimensions for achievement of pure tensile strain (Figure 2.4). Thus, specimen thinning can be achieved since there is no lateral thinning [8]. A uniaxial experiment test set-up can be seen in Figure 2.5.

Figure 2.4: Test specimen outline depicted for uniaxial tension test [8]

Figure 2.5: Uniaxial experiment test set-up designed for elastomers [8]

Only uniaxial tension test can not give enough information about free energy function. Thus, compression test also must be performed. However, in uniaxial compression test, homogenous deformation can not be obtained because of friction in compression areas in rubber materials. Thus, equibiaxial tension test is performed instead of uniaxial compression test. When straining is performed radially to the elastomer specimen in all directions in a single plane, free surfaces come together. In equibiaxial tension test, a state of strain equivalent to compression test is provided by performing an equal biaxial extension of a specimen. In spite of equibiaxial tension test's having more complexity than compression test, achievement of a pure state of strain will lead to have a better accuracy in material model [8]. An equibiaxial test specimen can be seen in Figure 2.6.

Figure 2.6: Test specimen producted for equibiaxial tension test [8]

As it is seen from Figure 2.6, radial cuts exist into specimen so that no tangential forces occur between the grips. An equibiaxial experiment test set-up can be seen in Figure 2.7.
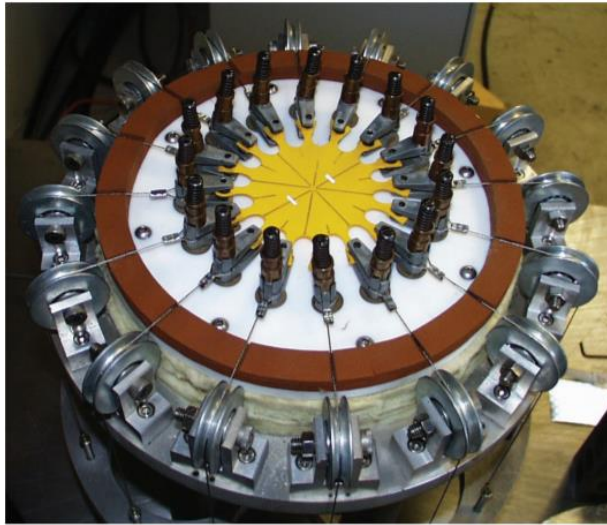
Figure 2.7: Equibiaxial experiment test set-up designed for elastomers [8]

Especially in deformations where I_1 and I_2 are small $(I_1, I_2 < 4)$, experimental errors get higher. In this situation, material parameters can be identified by pure shear test to minimize errors [9]. Moreover, since the rubber materials are assumed as incompressible, existence of pure shear is observed in the specimen at a 45 degree angle to the stretching direction. The key point in this experiment is that the specimen in the direction of stretching must be much shorter than the width. Thus, thinning of all the specimen can be achieved in the thickness direction by constraining the specimen perfectly in the lateral direction [8]. Pure shear test specimen outline can be seen below (Figure 2.8).
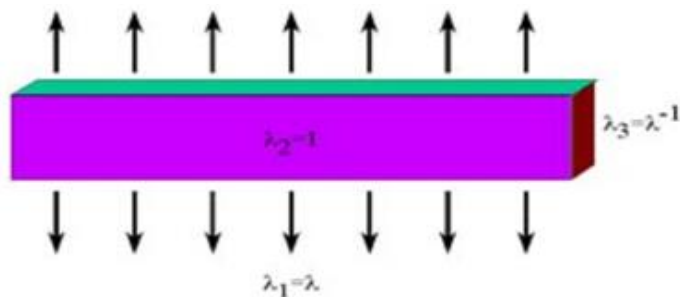
Figure 2.8: Test specimen outline depicted for pure shear test [8]

14

Moreover, a pure shear experiment test set-up can be seen in Figure 2.9.
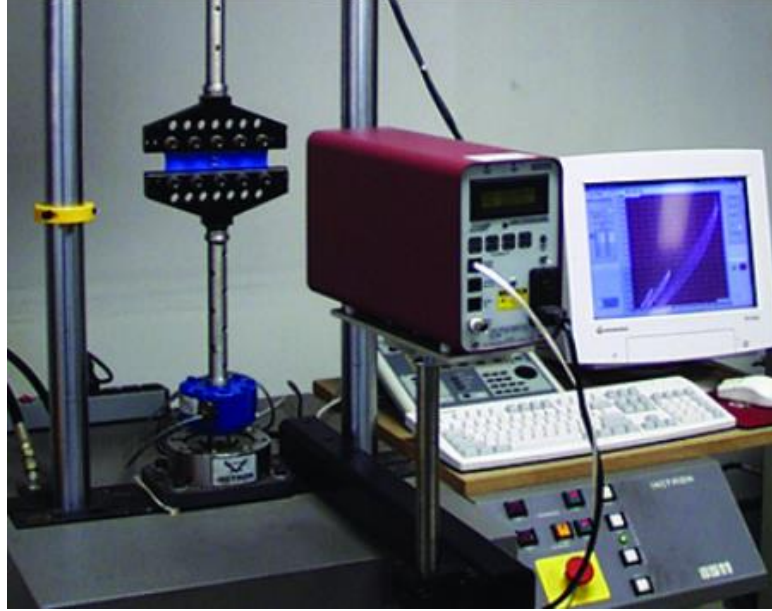
Figure 2.9: Pure shear experiment test set-up designed for elastomers [8]

For parameter identification of rubber models, Treloar data are used for uniaxial, equibiaxial and pure shear cases. In biaxial tension, the material is stretched from two orthogonal directions with different ratios. Equibiaxial tension case is specific form of biaxial tension case where the specimen is stretched equally from orthogonal directions. For biaxial case, Kawabata data are used for identification of material parameters.

According to test method, the deformation gradient, **F**, finger tensor, **B**, and stresses change. Kirchhoff stress is used in this point. First deformation mode was uniaxial tension. For uniaxial tension, related tensors can be found as

$$
[\mathbf{F}]_{ij} = \begin{bmatrix} \lambda & 0 & 0 \\ 0 & \frac{1}{\sqrt{\lambda}} & 0 \\ 0 & 0 & \frac{1}{\sqrt{\lambda}} \end{bmatrix}, \quad [\mathbf{B}]_{ij} = \begin{bmatrix} \lambda^2 & 0 & 0 \\ 0 & \frac{1}{\lambda} & 0 \\ 0 & 0 & \frac{1}{\lambda} \end{bmatrix}, \quad [\boldsymbol{\tau}]_{ij} = \begin{bmatrix} \tau & 0 & 0 \\ 0 & 0 & 0 \\ 0 & 0 & 0 \end{bmatrix}. \tag{2.32}
$$

Here λ is known. Due to incompressible case, λ_2 and λ_3 are equal to $\frac{1}{\sqrt{\lambda}}$. The stress occurring on stretching direction is unknown. Principal invariants can be found according to equations (2.14), (2.15) and (2.16). As it is stated above, $I_3=1$ because of incompressibility. Principal invariants can be calculated as

$$I_1 = \lambda^2 + \frac{2}{\lambda},$$
(2.33)

$$I_2 = 2\lambda + \frac{1}{\lambda^2},$$
(2.34)

$$I_3 = 1.$$
(2.35)

Second deformation mode was equibiaxial tension. In this case, related tensors can be written as

$$[\mathbf{F}]_{ij} = \begin{bmatrix} \lambda & 0 & 0 \\ 0 & \lambda & 0 \\ 0 & 0 & \frac{1}{\lambda^2} \end{bmatrix}, \quad [\mathbf{B}]_{ij} = \begin{bmatrix} \lambda^2 & 0 & 0 \\ 0 & \lambda^2 & 0 \\ 0 & 0 & \frac{1}{\lambda^4} \end{bmatrix}, \quad [\boldsymbol{\tau}]_{ij} = \begin{bmatrix} \tau_1 & 0 & 0 \\ 0 & \tau_2 & 0 \\ 0 & 0 & 0 \end{bmatrix}.$$
(2.36)

Here, τ_1 and τ_2 are unknown. Similiarly, due to incompressibility, deformation gradient and finger tensor are written. Principal invariants in this case can be found as

$$I_1 = 2\lambda^2 + \frac{1}{\lambda^4},$$
(2.37)

$$I_2 = \lambda^4 + \frac{2}{\lambda^2},$$
(2.38)

$$I_3 = 1.$$
(2.39)

For pure shear deformation, related tensors can be written as

16

$$[\mathbf{F}]_{ij} = \begin{bmatrix} \lambda & 0 & 0 \\ 0 & 1 & 0 \\ 0 & 0 & \frac{1}{\lambda} \end{bmatrix}, \quad [\mathbf{B}]_{ij} = \begin{bmatrix} \lambda^2 & 0 & 0 \\ 0 & 1 & 0 \\ 0 & 0 & \frac{1}{\lambda^2} \end{bmatrix}, \quad [\boldsymbol{\tau}]_{ij} = \begin{bmatrix} \tau_1 & 0 & 0 \\ 0 & \tau_2 & 0 \\ 0 & 0 & 0 \end{bmatrix}. \tag{2.40}$$

In pure shear case, since one direction is kept unstretched, the stretch is 1 (one) on this direction. Here, τ_1 and τ_2 are also unknown. Similiarly, due to incompressibility, deformation gradient and finger tensor are formed. Principal invariants in this case can be found as

$$I_1 = \lambda^2 + 1 + \frac{1}{\lambda^2}, \tag{2.41}$$

$$I_2 = \lambda^2 + 1 + \frac{1}{\lambda^2}, \tag{2.42}$$

$$I_3 = 1. \tag{2.43}$$

For biaxial tension case, related matrices can be written as

$$[\mathbf{F}]_{ij} = \begin{bmatrix} \lambda_1 & 0 & 0 \\ 0 & \lambda_2 & 0 \\ 0 & 0 & \frac{1}{\lambda_1 \lambda_2} \end{bmatrix}, [\mathbf{B}]_{ij} = \begin{bmatrix} \lambda_1{}^2 & 0 & 0 \\ 0 & \lambda_1{}^2 & 0 \\ 0 & 0 & \frac{1}{\lambda_1{}^2 \lambda_1{}^2} \end{bmatrix}, [\boldsymbol{\tau}]_{ij} = \begin{bmatrix} \tau_1 & 0 & 0 \\ 0 & \tau_2 & 0 \\ 0 & 0 & 0 \end{bmatrix}. \tag{2.44}$$

In biaxial case, the material is stretched from two orthogonal directions which leads to different stretches. λ_1 and λ_2 are known. Here, τ_1 and τ_2 are also unknown. Similarly, due to incompressibility, deformation gradient and finger tensor are formed. Principal invariants in this case can be found as

$$I_1 = \lambda_1{}^2 + \lambda_2{}^2 + \frac{1}{\lambda_1{}^2 \lambda_2{}^2}, \tag{2.45}$$

$$I_2 = \lambda_1{}^2 \lambda_2{}^2 + \frac{1}{\lambda_2{}^2} + \frac{1}{\lambda_1{}^2}, \tag{2.46}$$

$$I_3 = 1. \tag{2.47}$$

2.2. Literature Study

In this thesis, ten rubber hyperelastic models are examined. Seven of them are phenomenological models. Those are Neo Hooke [10], Mooney [11], Carroll [12], Shariff [13], Ogden [14], Biderman [15] and Yeoh [16] models. Three of the hyperelastic models are micro-mechanical models. Those are microsphere model [17], eight-chain model [18] and extended tube model [19]. Details of these models will be given in the next chapter.

The efficiency of ten hyperelastic models which are stated above are compared in this thesis. Related calculations are performed in MATLAB GUI. Thus, this study is a comparative study. Previous comparative studies have been conducted to identify the material parameter sets in related models. There are also studies about parameter identification of one hyperelastic model. In the accessible literature, similar studies are investigated and those studies will be reviewed in this section. The attention will be drawn to studies about parameter identification of hyperelastic models.

Marckmann and Verron [3] proposed a comparative study through twenty hyperelastic rubber models. They used two classical sets of experimental data (Treloar and Kawabata data) in different types of loading conditions. They proposed an efficient fitting procedure to identify material parameters. Moreover, stretch range of validity of each model are determined for each model. Like this thesis, rubber material models with their related definitions and calculations are given. Similarly, both phenomenological models and micro-mechanical models are presented in this study. As fitting procedure, least square method is used.

Steinmann, Hossain and Possart [20] reviews fourteen hyperelastic rubber models. Stress-stretch relations for certain deformation modes are derived. Moreover, efficiencies of those models are evaluated by using classical Treloar data. In this study, uniaxial, equibiaxial and pure shear deformation modes are evaluated. In fitting procedure, four different material parameter sets are defined. Those are

uniaxial fitted, equibiaxial fitted, pure shear fitted and three deformation modes together fitted material parameter sets.

Seibert and Schöche [21] also propose a comparative study by using six different hyperelastic models. In this comparison study, uniaxial and biaxial data of a carbon black-filled rubber are used. It is concluded that using higher order terms lead to achieve typical increase in stiffness at large strains. It is also stated that Arruda-Boyce model gives reliable predictions with biaxial deformation even though the material parameter set which are found by fitting with only uniaxial data is used.

Arruda and Boyce [22] also reviewed several models using Treloar's experimental data for uniaxial, equibiaxial and pure shear deformation modes. In this study, statistical mechanical treatments, invariant based continuum mechanics treatments and stretch based continuum mechanics treatments are presented. It is also stated that the effects of incompressibility are significant in certain applications. Thus, appropriate extension of the strain energy functions is needed in those applications.

Rackl [23] provided a technical background for curve fitting of Ogden, Yeoh and polynomial model. The least squares method is used for curve fitting procedure. The results are compared with the parameters found in ANSYS.

Ali, Hosseini and Sahari [24] reviewed different constitutive models for rubber- like materials. In this study, polynomial, reduced polynomial, Ogden, Mooney-Rivlin, Neo-Hooke, Yeoh, Arruda-Boyce and Van der Waals models are reviewed. Least square optimization method is offered to determine material parameters. It is stated that material parameter identification is significant to have the relation between stress and strain because it is needed for finite element analysis of rubber materials. Finally, it is stated that classification of the models depends on domain of validity for all modes of deformation, number of material parameters and the type of formulation.

Wu, Li and Wang [25] used Levenberg-Marquardt nonlinear optimization algorithm to determine the material parameters of Ogden model for uniaxial tension, biaxial tension, planar tension and simple shear by using Treloar experimental data. Those results are compared with ANSYS results for numerical verification. Number of terms considered for Ogden model are set as 3 (three) and 4 (four). The results are given for those options. When the number of terms is taken as 3 (three), the capability of fitting is stated as very well. If it is taken as 4 (four), the results are best.

Nowak [26] also aimed to determine the phenomenological model for polyurethane (PUR) rubbers used in civil engineering. Stress-strain relation is characterized and the behavior of PUR rubbers is simulated. After strain-energy function is established, Piola-Kirchhoff stress is obtained. Then, parameter identifications of model parameters are presented. Identification process is supported by the experimental data from uniaxial quasi-static tension and compression tests. Material behavior is examined for both incompressible and slightly compressible deformations.

Attard and Hunt [27] presented a different comparative study by using seven different authors' experimental data to show efficiency of their own model for uniaxial tension, equibiaxial tension, pure shear, compression and biaxial extension. A higher elasticity model which is composed of a Neo-Hookean-like compressible and a generalized Mooney-type incompressible component is proposed in their study.

CHAPTER 3

HYPERELASTIC MODELS STRESS-STRETCH EXPRESSION CALCULATIONS

As it was stated before, stress-stretch expressions of rubbers can be written by using free energy functions and this is the starting point for rubber material modeling. It is assumed that materials show isotropic and incompressible behavior. In the fully incompressible limit, free energy function can be written as

$$W = W(\mathbf{C}) = \widetilde{W}(\mathbf{F}) = \widehat{W}(\mathbf{B}). \qquad (3.1)$$

That means that free energy functions can be written according to certain tensors. Since rubber materials shows a decoupled response to volumetric and isochoric deformations, it should be written as

$$W(\mathbf{C}) = W_{vol}(J) + W_{iso}(\bar{\mathbf{C}}). \qquad (3.2)$$

$\bar{\mathbf{C}}$ is the isochoric right Cauchy-Green tensor and can be calculated as

$$\bar{\mathbf{C}} = J^{-2/3}\mathbf{C}. \qquad (3.3)$$

Second Piola-Kirchhoff stress can be written according to isochoric free energy function as

$$\mathbf{S} = 2\,\partial_{\mathbf{C}}\,W. \qquad (3.4)$$

This tensor also can be decomposed into volumetric and isochoric parts as

$$\mathbf{S} = 2\frac{\partial W_{vol}}{\partial \mathbf{C}} + 2\frac{\partial W_{iso}}{\partial \mathbf{C}}. \qquad (3.5)$$

Volumetric part can be written as

$$\mathbf{S_{vol}} = 2\frac{\partial W_{vol}(J)}{\partial J}\frac{\partial J}{\partial \mathbf{C}} = \widehat{p}\,\mathbf{C}^{-1}. \tag{3.6}$$

Here $\widehat{p}$ is hydrostatic pressure term and defined as

$$\widehat{p} = J\frac{\partial W_{vol}(J)}{\partial J}. \tag{3.7}$$

In this study, materials are assumed as isotropic and incompressible. Thus, in the case of incompressibility J=1, $\widehat{p}$ serves as a Lagrange multiplier [20]. Then, the second Piola-Kirchhoff stress becomes

$$\mathbf{S} = \widehat{p}\,\mathbf{C}^{-1} + 2\frac{\partial W_{iso}}{\partial \mathbf{C}}. \tag{3.8}$$

It was also stated before that Kirchhoff stress is the push forward of the second Piola-Kirchhoff stress tensor in (2.31) equation. Thus, if we substitute equation (3.8) into (2.31) equation, the expression is obtained as

$$\boldsymbol{\tau} = \mathbf{F}(\widehat{p}\,\mathbf{C}^{-1} + 2\frac{\partial W_{iso}}{\partial \mathbf{C}})\mathbf{F}^{T}. \tag{3.9}$$

Here, Kirchhoff stress is obtained. After necessary calculations, it can be written as

$$\boldsymbol{\tau} = \widehat{p}\,\mathbf{1} + \widehat{\boldsymbol{\tau}}. \tag{3.10}$$

Here $\widehat{\boldsymbol{\tau}}$ is isochoric Kirchhoff stress and can be written as

$$\widehat{\boldsymbol{\tau}} = \mathbf{F}\left(2\frac{\partial W_{iso}}{\partial \mathbf{C}}\right)\mathbf{F}^{T} = \mathbf{F}\left(2\frac{\partial W_{iso}}{\partial \mathbf{B}}\right)\mathbf{F}^{T}. \tag{3.11}$$

Finally, the first Piola-Kirchhoff stress tensor can be calculated as

$$\mathbf{P} = \boldsymbol{\tau}\mathbf{F}^{-T}. \tag{3.12}$$

The pressure term $\hat{p}$ has to be calculated from equilibrium condition. Stress definitions for each material model can be obtained by using stress equations given above.

Isochoric Kirchhoff stress expression is given in equation (3.11). If we substitute (2.1) into this equation, the expression is obtained as

$$\hat{\boldsymbol{\tau}} = 2\mathbf{F}(\partial_{\mathbf{B}} \, W_{iso})\mathbf{F}^{T} = 2\mathbf{B}\frac{\partial W_{iso}(I_1, I_2)}{\partial \mathbf{B}} \, . \tag{3.13}$$

If this expression is written more detailed, isochoric Kirchhoff stress is obtained as

$$\hat{\boldsymbol{\tau}} = 2\mathbf{B}\frac{\partial_{\mathbf{B}} \, W_{iso}(I_1, I_2)}{\partial \mathbf{B}} = 2\mathbf{B}\left[\frac{\partial W_{iso}}{\partial I_1}\frac{\partial I_1}{\partial \mathbf{B}} + \frac{\partial W_{iso}}{\partial I_2}\frac{\partial I_2}{\partial \mathbf{B}}\right], \tag{3.14}$$

$$\text{where} \quad \frac{\partial I_1}{\partial \mathbf{B}} = \mathbf{1} \text{ and } \frac{\partial I_2}{\partial \mathbf{B}} = I_1\mathbf{1} - \mathbf{B} \, . \tag{3.15}$$

If we substitute equations (3.15) into equation (3.14), Kirchhoff stress becomes

$$\hat{\boldsymbol{\tau}} = 2\mathbf{B}\left[\frac{\partial W_{iso}}{\partial I_1}\mathbf{1} + \frac{\partial W_{iso}}{\partial I_2}(I_1\mathbf{1} - \mathbf{B})\right]. \tag{3.16}$$

So, Kirchhoff stress expression for invariant base formulation is obtained. Some hyperelastic rubber models have functional models in terms of principal stretches. Then, isochoric free energy function has the form as

$$W_{iso} = W_{iso}(\lambda_1^2, \lambda_2^2, \lambda_3^2). \tag{3.17}$$

The Kirchhoff stress tensor obtained for principal stretch-based formulation for purely incompressible materials is shown as

$$\boldsymbol{\tau} = \sum_{a=1}^{3} W_{iso,\lambda_a}\lambda_a\mathbf{n}_A\otimes\mathbf{n}_A + \hat{p}\,\mathbf{1} \, . \tag{3.18}$$

23

The derivatives of isochoric free energy function, W_{iso}, with respect to principal stretches are used in this formulation. As it is seen from above, isochoric free energy function definition is required for both phenomenological and micro-mechanical models.

3.1. Phenomenological Models

Phenomenological models can be principal strain invariants based and principal stretch-based formulations. The most general case for isochoric free energy function based on principal strain invariants is defined as

$$W_{iso} = \sum_{k,l=0}^{\infty} c_{kl} \, (I_1 - 3)^k (I_2 - 3)^l. \tag{3.19}$$

It must be noted that isotropic and incompressible case is assumed in all calculations [20]. Seven phenomenological models are presented in this thesis. Equation (3.19) represent most general case. Neo-Hooke, Mooney, Yeoh and Biderman models are in this form. Shariff and Carroll models are not in this form. Ogden model has a stretch-based formulation.

3.1.1. Neo-Hooke Model

Neo-Hooke model [10] is the simplest case of equation (3.19). In this model, k is taken as 1 (one) and l is taken as 0 (zero). It is also assumed that C_{00}=0. The isochoric free energy function of Neo-Hooke model is given as

$$W_{iso} = \frac{\mu}{2} (I_1 - 3). \tag{3.20}$$

Here, μ=$2c_{10}$. μ is called as shear modulus.

The derivatives of free energy function with respect to first and second principal strain invariants are given as

$$\frac{\partial W_{iso}}{\partial I_1} = \frac{\mu}{2}, \qquad \frac{\partial W_{iso}}{\partial I_2} = 0. \tag{3.21}$$

Finger tensor, **B**, can be found according to deformation mode. Thus, isochoric Kirchhoff stress definition is obtained which is given in equation (3.14). Kirchhoff stress is found according to equation (3.10). Here, Kirchhoff stress tensor differs according to deformation mode as it was stated before in Section (2.1.3). After Kirchhoff stress is obtained, the first Piola-Kirchhoff stress is found by using the equation (3.12).

All those calculations for each hyperelastic models are done in MATLAB. The detailed information about algorithm used in MATLAB will be discussed in the next chapter. Neo-Hooke model has only one material parameter, μ. Neo-Hooke model can give acceptable results only for small deformations ($\lambda<1.5$) since it does not have enough parameters and powers of strain invariants to have 'S' shape. This will be proved in the results and discussion. Moreover, Neo-Hooke model provides a relation to micro-mechanical approaches by using Gaussian chain statistics. Thus, it coincides with 3 (three) chain model.

3.1.2. Mooney Model

In Mooney Model [11], k=1 and l=1 in equation (3.19). It is assumed that $C_{00}=0$ and $C_{11}=0$. Thus, the isochoric free energy function of Mooney model is written as

$$W_{iso} = C_1(I_1 - 3) + C_2(I_2 - 3). \qquad (3.22)$$

Here, C_1 and C_2 are material parameters. Mooney model is suitable only in small stretches. The difference between Mooney model and Neo-Hooke model is Mooney model's having second principal invariant in its isochoric free energy function. This will be discussed in results and discussion parts. The derivatives of free energy function with respect to first and second principal strain invariants are found as

$$\frac{\partial W_{iso}}{\partial I_1} = C_1, \qquad \frac{\partial W_{iso}}{\partial I_2} = C_2. \qquad (3.23)$$

To find the stress tensors, the same procedure stated in Neo-Hooke model is applied

in MATLAB toolbox.

3.1.3. Biderman Model

In this model [15], first and second principal invariants are used in free energy function like in Mooney model. However, the difference is that second and third powers of I_1 terms are used in the isochoric free energy function as

$$W_{iso} = C_{10}(I_1 - 3) + C_{01}(I_2 - 3) + C_{20}(I_1 - 3)^2 + C_{30}(I_1 - 3)^3. \qquad (3.24)$$

There are four material parameters in this model. The derivatives of free energy function with respect to first and second principal strain invariants are found as

$$\frac{\partial W_{iso}}{\partial I_1} = C_{10} + 2C_{20}(I_1 - 3) + 3C_{30}(I_1 - 3)^2, \qquad \frac{\partial W_{iso}}{\partial I_2} = C_{01}. \quad (3.25)$$

To find the stress tensors, the same procedure stated in Neo-Hooke model is applied in MATLAB toolbox.

3.1.4. Yeoh Model

Yeoh model [16] uses only I_1 term. However, I_1 terms up to power of 3 (three) are included. Since it is observed in experiments that filled elastomers give almost 0 (zero) values for $\frac{\partial W_{iso}}{\partial I_2}$, this model is proposed especially for those rubbers. The isochoric free energy function of Yeoh model is given as

$$W_{iso} = C_1(I_1 - 3) + C_2(I_1 - 3)^2 + C_3(I_1 - 3)^3. \qquad (3.26)$$

C_1, C_2 and C_3 are material parameters in this model. The derivative of free energy function with respect to first principal strain invariant is given as

$$\frac{\partial W_{iso}}{\partial I_1} = C_1 + 2C_2(I_1 - 3) + 3C_3(I_1 - 3)^2, \qquad \frac{\partial W_{iso}}{\partial I_2} = 0. \quad (3.27)$$

Thus, it can be easily seen that the isochoric free energy function of Yeoh model does not have only I_2 term if it is compared to Biderman Model. The effect of I_2 term will be seen in the results.

To find the stress tensors, the same procedure stated in Neo-Hooke model is applied in MATLAB toolbox.

3.1.5. Carroll Model

In Carroll Model [12], I_1 term with power of four and square root of I_2 terms are used to decrease the error. It is based on a successive extension of free energy function by reducing the errors remaining in the response of previous terms. The first step is fitting a Neo-Hookean function with Treloar uniaxial tension data. Remaining difference is fitted once more with $(I_1)^4$ term. First and second term together provides simulating equibiaxial tension. Finally, deviation from equibiaxial Treloar data are approached by using the $\sqrt{I_2}$ term [20]. The isochoric free energy function of Carroll model is given as

$$W_{iso} = aI_1 + b(I_1)^4 + c\sqrt{I_2}. \tag{3.28}$$

a, b and c are material parameters in this function. The derivatives of free energy function with respect to first and second principal invariants are found as

$$\frac{\partial W_{iso}}{\partial I_1} = a + 4b(I_1)^3, \qquad \frac{\partial W_{iso}}{\partial I_2} = \frac{c}{2}(I_2)^{-0.5}. \tag{3.29}$$

To find the stress tensors, the same procedure stated in Neo-Hooke model is applied in MATLAB toolbox.

3.1.6. Ogden Model

Ogden model [14] is a principal stretch-based formulation. Thus, the stress calculations are done according to equation (3.18). The isochoric free energy function of Carroll Model is given as

$$W_{iso} = \sum_{k=1}^{K} \frac{\mu_k}{\alpha_k} \left[\bar{\lambda}_1{}^{\alpha_k} + \bar{\lambda}_2{}^{\alpha_k} + \bar{\lambda}_3{}^{\alpha_k} - 3 \right]. \tag{3.30}$$

Here, modified principal stretches are used. However, it is same with principal stretch in incompressible case. If K number is taken bigger, the calculations will be more complex. A moderate K number should be used for calculations. In this thesis, K is taken as 3 (three). It should be also noted that material parameters should provide the stability condition as

$$\mu_k \alpha_k > 0, \quad \text{for } k = 1,2 \text{ and } 3. \tag{3.31}$$

3.1.7. Shariff Model

Shariff model [13] differs from other phenomenological models by proposing a new model which has linear parameters proposed with a general separable form given as

$$S(\lambda_1, \lambda_2, \lambda_3) = r(\lambda_1) + r(\lambda_2) + r(\lambda_3). \tag{3.32}$$

Thus, parameter identification process can be done by solving linear equations. Some researchers proposed separable strain energy functions like in the form of equation (3.32). However, those functions are nonlinear in their parameters. One of Shariff model's parameters is E (Young's Modulus). Cauchy stress can be obtained by the relation of separable strain energy function as

$$\sigma_i = \lambda_i \frac{\partial S}{\partial \lambda_i} - \hat{p}. \tag{3.33}$$

Here, $\hat{p}$ is hydrostatic pressure which occurs due to incompressibility assumption. Here, i=1,2,3. From equation (3.33), the following expression can be obtained as

$$\sigma_1 - \sigma_2 = \lambda_1 \frac{\partial W_{iso}}{\partial \lambda_1} - \lambda_2 \frac{\partial W_{iso}}{\partial \lambda_2}. \tag{3.34}$$

Simplification for equation (3.34) can be done as

28

$$\sigma_1 - \sigma_2 = \lambda_1 r'(\lambda_1) - \lambda_2 r'(\lambda_2). \tag{3.35}$$

Prime in the equation (3.35) shows the differentiation with respect to the argument of function. A restriction is done in this point by taking $r'(1)=0$ without loss of generality due to simplicity in r function. Then, for $\lambda_2 = 1$, equation (3.35) becomes

$$\sigma_1 - \sigma_2 = \lambda_1 r'(\lambda_1). \tag{3.36}$$

An extension is done for moderate and larger strains by following expression as

$$f(\lambda) = \lambda r'(\lambda) = E \sum_{i=0}^{n} \alpha_i \phi_i. \tag{3.37}$$

Here, E and α_i are material parameters. In this thesis, n=3. Thus, there are five parameters totally. According to this model, Cauchy stress can be found as

$$\sigma_1 = f(\lambda) - f\left(\frac{1}{\lambda^m}\right), \quad \text{where } m = \frac{1}{2}, 1 \text{ and } 2. \tag{3.38}$$

The assumption is that $\lambda=\lambda_1>1$. Here, m=1/2 for uniaxial tension case, 1 for pure shear deformation case and 2 for equibiaxial tension case. According to model, ϕ_0, ϕ_1, ϕ_2 and ϕ_3 are chosen as

$$\phi_0(\lambda) = \left(\frac{2\ln(\lambda)}{3}\right), \quad \phi_1(\lambda) = e^{(1-\lambda)} + \lambda\text{-2,}$$

$$\phi_2(\lambda) = e^{(1-\lambda)}\text{-}\lambda \text{ and } \phi_3(\lambda) = \frac{(\lambda - 1)^3}{\lambda^{3.6}}. \tag{3.39}$$

For biaxial deformation case the calculations are given as

$$\sigma_b = \sigma_1 - \sigma_2 = f(\lambda) - f(\lambda_2). \tag{3.40}$$

Also, it must be noted that the stress, σ_1, in a uniaxial or equibiaxial or a pure shear deformation mode has a relation with the biaxial stress, σ_b, if the material can be written by a separable form of strain energy function. It can be written as

$$\sigma_b = \sigma_b(\lambda_0) - \sigma_b\left(\frac{1}{\lambda_0^m}\right). \qquad (3.41)$$

3.2. Micro-Mechanical Models

The microscopic response of chains in the network in rubber materials is the subject of micro-mechanical models. It is based on statistical mechanics arguments on networks of idealized chain molecules. Computational costs of micro-mechanical models are generally bigger than phenomenological models. However, micro-mechanical models provide to relate macroscopic mechanical behavior to physical and chemical structure at molecular level. Thus, micro-mechanical models have got more attention recently.

The rubber structure is modeled as a chain of N rigid beams with length L. The beams are called as Kuhn segments. Each segment has multiple monomers. According to statistical approaches, distance of a stress free undeformed chain is calculated as

$$r_0 = \sqrt{N}L. \qquad (3.42)$$

From here, chain stretch can be calculated as

$$\Lambda = \frac{r}{r_0}. \qquad (3.43)$$

Here, r is the distance of the deformed chain.

Thus, scalar free energy function should be written as a function of Λ which can be shown as $W = W(\Lambda)$. Free energy function of Gauss chain is one of the important examples and it can be calculated as

$$W^{\text{Gauss}}(\Lambda) = \frac{3}{2} k_b \Theta \Lambda^2 + W_0. \qquad (3.44)$$

The other important example is free energy function of Langevin chain. It can be calculated as

$$W^{\text{Langevin}}(\Lambda) = k_b \Theta N \left[\frac{\Lambda}{\sqrt{N}} \mathcal{L}^{-1} \left(\Lambda \sqrt{N^{-1}} \right) + \ln \left(\frac{\mathcal{L}^{-1}\left(\Lambda \sqrt{N^{-1}} \right)}{\sinh \left(\mathcal{L}^{-1}\left(\Lambda \sqrt{N^{-1}} \right) \right)} \right) \right]. \quad (3.45)$$

Where k_b, Θ and $\mathcal{L}^{-1}$ are denoted as Boltzmann's constant, absolute temperature and inverse of Langevin function respectively. It should be noted that Gaussian chain is more suitable for low to moderate stretches. Also, inverse of Langevin function is generally substituted by using Pade approximation [28] as

$$\gamma = \mathcal{L}^{-1}(\Lambda N^{-1}) \approx \Lambda \sqrt{N^{-1}} \frac{3N - \Lambda^2}{N - \Lambda^2}. \qquad (3.46)$$

Those Gauss and Langevin chain free energy expressions are written for free energy function of individual chains. The free energy of a whole network is equal to the sum of the free energy of individual chains. For this purpose, ensemble averaging of chain energies are used. Thus, mechanical behavior of true polymer network can be realized as much as possible by using the isochoric free energy function shown as

$$W_{\text{iso}} = W_{\text{iso}}(\bar{\mathbf{C}}) = \frac{n}{K} \sum_{k=1}^{K} W(\Lambda_k). \qquad (3.47)$$

Different chain structure models were proposed by various researchers. In this thesis, three of them are examined [20].

3.2.1. Eight Chain Model

This model is proposed by Arruda and Boyce [18]. A distribution of chains with eight directions starting from a unit sphere in the center of a cubic and going to the corners of the cubic is the main idea of this model. Stretch of those diagonal chains govern the model (Figure 3.1).
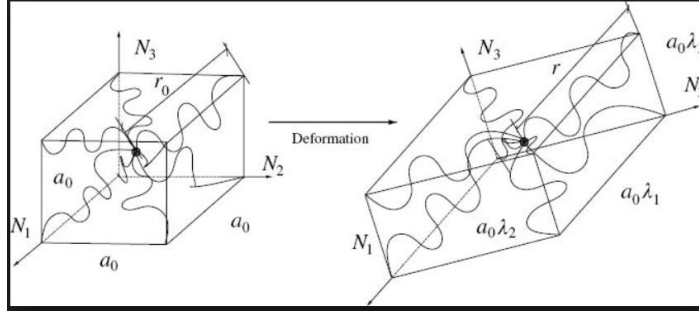

Figure 3.1: Eight-chain model structure undergoing deformation [29]

Chain stretch can be calculated for this model as

$$\Lambda = \Lambda_k = \frac{r_k}{r_0} = \frac{1}{\sqrt{3}} \sqrt{\lambda_1{}^2 + \lambda_2{}^2 + \lambda_3{}^2} . \tag{3.48}$$

Here k=1,…,8.

Isochoric free energy function of eight chain model by using equation (3.47) can be calculated as

$$W_{iso} = \frac{n}{8} \sum_{k=1}^{8} W^{Langevin}(\Lambda_k) = \mu N \left[\sqrt{N^{-1}} \Lambda \gamma + \ln\left(\frac{\gamma}{\sinh(\gamma)} \right) \right]. \tag{3.49}$$

Here, μ and N are material parameters of eight chain model. Isochoric Kirchhoff stress expression can be obtained as

$$\bar{\tau} = \frac{\mu}{3} \frac{9N - I_1}{3N - I_1} \mathbf{B} . \tag{3.50}$$

3.2.2. Extended Tube Model

Kaliske and Heinrich [19] proposed the extended tube model. This model is an extension of tube model of Kaliske and Heinrich. They proposed an inextensibility parameter δ and a new strain energy function is formed. In their research, not only limited chain extensibility of network chains but also topological constraints in filled rubbers are proposed. The isochoric free energy function of this model is given as

$$W_{iso} = \frac{G_c}{2}\left[\frac{(1-\delta^2)(D-3)}{1-\delta^2(D-3)} + \ln(1-\delta^2(D-3))\right] + \frac{2G_e}{\beta^2}\sum_{A=1}^{3}(\lambda_A^{-\beta} - 1). \quad (3.51)$$

G_c, β, G_e and δ are material parameters. G_c is modulus of chemical network nodes. G_e is modulus of topological constraints. δ is finite deformation of finite chains and β is relaxation of system deformations. It should be also noted that empirical parameter β should be between 0 and 1. D expression also can be found as

$$D = \sum_{A=1}^{3}\lambda_A^2 = \lambda_1^2 + \lambda_2^2 + \lambda_3^2 = I_1. \quad (3.52)$$

If we take δ parameter as zero, the energy function becomes

$$W_{iso} = \frac{G_c}{2}[I_1 - 3] + \frac{2G_e}{\beta^2}\sum_{A=1}^{3}(\lambda_A^{-\beta} - 1). \quad (3.53)$$

A transition can be done by inserting $I_1 = \lambda_1^2 + \lambda_2^2 + \lambda_3^2$, $\alpha_1 = 2$, $\alpha_2 = -\beta$, $\mu_1 = G_c$, $\mu_2 = \frac{-2}{\beta}G_e$. Thus, Ogden model is achieved as

$$W_{iso} = \sum_{k=1}^{K}\frac{\mu_k}{\alpha_k}[\lambda_1^{\alpha_k} + \lambda_2^{\alpha_k} + \lambda_3^{\alpha_k} - 3]. \quad (3.54)$$

Here K=2.

3.2.3. Microsphere Model

In microsphere model which is proposed by Goktepe [17], the chains are distributed in a unit sphere. The single chain has two micro-kinematic variables: the stretch λ and area contraction v (Figure 3.2).

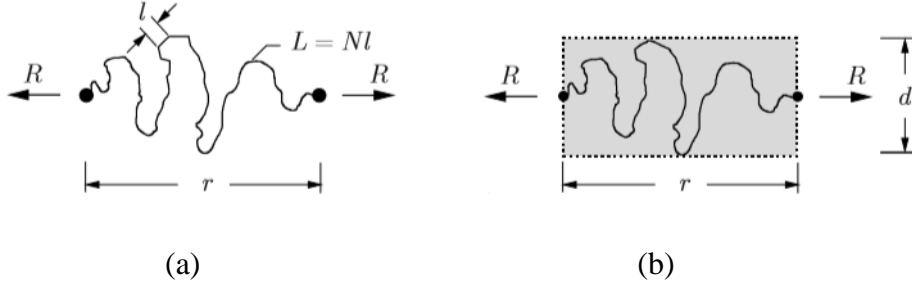(a)   (b)

Figure 3.2: Single chain outline of microsphere model: (a) Free single chain consisting of N segments with length l (b) Straight tube diameter constraining chain topology [17]

Area contraction can be calculated as

$$v = \left(\frac{d_0}{d}\right)^2 .$$
(3.55)

Here d is the deformed tube diameter and d_0 is the undeformed tube diameter.

Free energy function of this model is decoupled into two parts for two micro-kinematic variables as

$$W = W_f + W_c .$$
(3.56)

Where W_f is free energy function for stretch part and W_c is free energy function for area contraction part. Free energy function for stretch part can be calculated by using Langevin function given in equation (3.45) for one single chain. Free energy function for area contraction part for one single chain can be calculated as

$$W_c = k_b \Theta NUv + W_0 \,. \tag{3.57}$$

Where U is tube geometry parameter and can be calculated as

$$U = \alpha \left(\frac{l}{d_0}\right)^2 . \tag{3.58}$$

Here α changes according to the shape of the cross section of the tube. In non-affine transformation, parallel lines of body are not kept as parallel after deformation. Non-affine model is developed in this model by letting micro-stretches fluctuate around macro-stretches. In this manner, the p root average of the non-affine stretch λ is taken as equal to the p root average of the macroscopic stretch $\bar{\lambda}$ as

$$\bar{\lambda}_i = \sqrt{r_i . \bar{C} r_i} \,, \tag{3.59}$$

$$\lambda = \left(\frac{1}{|S|} \int \bar{\lambda}^p \, dA\right)^{1/p} . \tag{3.60}$$

Here S is sphere surface and p is non-affine stretch parameter. Integration is performed over the surface of unit sphere. Discrete integration over sphere is applied instead of integration over the surface of unit sphere.

Non-affine tube part is developed by defining a fictitious straight micro-tube which constrains free movement of single chain. Non-affine stretch parameter q relates the microscopic tube contraction v and macroscopic area change as

$$\bar{v}_i = \sqrt{r_i . \bar{C}^{-1} r_i} \text{ and} \tag{3.61}$$

$$v = \bar{v}_i{}^q . \tag{3.62}$$

In non-affine microsphere model, isochoric Kirchhoff stress is calculated as

$$\bar{\tau} = \tau_f \lambda^{1-p} \mathbf{h} - \mu NU \mathbf{k} \,. \tag{3.63}$$

Material parameters are N, μ, U, q and p. τ_f is micro-stress. N is number of chain segments and μ is shear modulus like in the other micro-mechanical models. **h** and **k** tensors will be defined in more detail below.

In this model, calculations for non-affine microsphere model is given systematically. First step is to calculate the unimodular part of deformation gradient as

$$\bar{\mathbf{F}} = J^{-1/3}\mathbf{F}.$$

(3.64)

Unimodular part of deformation gradient is equal to deformation gradient in incompressibility case. Then, set of orientation vectors and associated weight factors are set. The chains are distributed nearly uniformly by using these factors.

Discrete points are defined only for the half-sphere. 21 integration points for the half sphere as

$$\mathbf{r}^i = r_1^i \mathbf{e}_1 + r_2^i \mathbf{e}_2 + r_3^i \mathbf{e}_3.$$

(3.65)

Microstructure of the network model is described by stereographic pole projection of unit sphere in Figure 3.3 with 21 integration points.
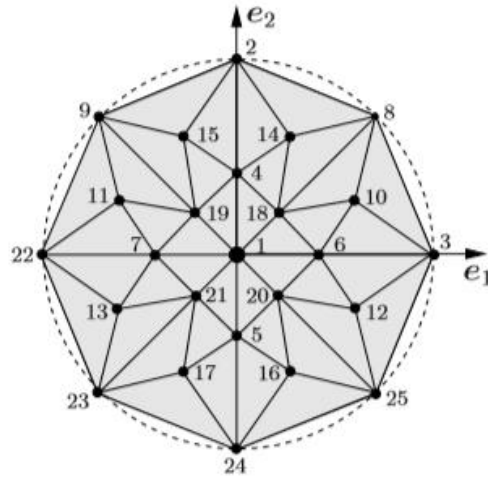

Figure 3.3: Stereographic pole projection of unit sphere describing the microstructure of the network model [17]

21 integration points and associated weights are given below in Table 3.1.

Table 3.1: Integration points and weights on unit sphere [16]

No	r_1^i	r_2^i	r_3^i	$w^i/2$
1	0	0	1	0.0265214244093
2	0	1	0	0.0265214244093
3	1	0	0	0.0265214244093
4	0	0.707106781187	0.707106781187	0.0199301476312
5	0	-0.707106781187	0.707106781187	0.0199301476312
6	0.707106781187	0	0.707106781187	0.0199301476312
7	-0.707106781187	0	0.707106781187	0.0199301476312
8	0.707106781187	0.707106781187	0	0.0199301476312
9	-0.707106781187	0.707106781187	0	0.0199301476312
10	0.836095596749	0.387907304067	0.387907304067	0.0250712367487
11	-0.836095596749	0.387907304067	0.387907304067	0.0250712367487
12	0.836095596749	-0.387907304067	0.387907304067	0.0250712367487
13	-0.836095596749	-0.387907304067	0.387907304067	0.0250712367487
14	0.387907304067	0.836095596749	0.387907304067	0.0250712367487
15	-0.387907304067	0.836095596749	0.387907304067	0.0250712367487
16	0.387907304067	-0.836095596749	0.387907304067	0.0250712367487
17	-0.387907304067	-0.836095596749	0.387907304067	0.0250712367487
18	0.387907304067	0.387907304067	0.836095596749	0.0250712367487
19	-0.387907304067	0.387907304067	0.836095596749	0.0250712367487
20	0.387907304067	-0.387907304067	0.836095596749	0.0250712367487
21	-0.387907304067	-0.387907304067	0.836095596749	0.0250712367487

Then, non-affine stretch and non-affine tube parts are calculated. The last step is to write superimposed stress response.

In non-affine stretch part micro and macro stresses, τ_f and $\bar{\boldsymbol{\tau}}_f$ can be obtained as

$$\tau_f = \mu \frac{(3N - \lambda^2)}{(N - \lambda^2)\lambda}, \tag{3.66}$$

$$\bar{\boldsymbol{\tau}}_f = \tau_f \lambda^{1-p} \mathbf{h}. \tag{3.67}$$

Here $\mathbf{h}$ and λ can be obtained as

$$\mathbf{h} = \sum_{i=1}^{m} (\bar{\lambda}^i)^{p-2} \mathbf{t}^i \otimes \mathbf{t}^i w^i, \tag{3.68}$$

$$\lambda = \left[\sum_{i=1}^{m} (\bar{\lambda}^i)^p \, w^i \right]^{1/p}. \tag{3.69}$$

Here, deformed tangents $\mathbf{t}^i = \bar{\mathbf{F}} \mathbf{r}^i$ and affine micro stretches $\bar{\lambda}^i = |\mathbf{t}^i|$. Equation (3.69) is obtained by performing discrete integration to equation (3.60).

In non-affine tube part, macro stresses can be computed as

$$\bar{\boldsymbol{\tau}}_c = \mu N U \mathbf{k}. \tag{3.70}$$

Here k can be computed as

$$\mathbf{k} = q \sum_{i=1}^{m} (\bar{v}^i)^{q-2} \mathbf{n}^i \otimes \mathbf{n}^i w^i. \tag{3.71}$$

Here, deformed normal $\mathbf{n}^i = \bar{\mathbf{F}}^{-T} \mathbf{r}^i$ and $\bar{v}^i = |\mathbf{n}^i|$.

Finally, superimposed stress response can be written by adding macro-stresses of stretch and tube deformation parts as

$$\bar{\boldsymbol{\tau}} = \bar{\boldsymbol{\tau}}_c + \bar{\boldsymbol{\tau}}_f. \tag{3.72}$$

Thus, equation (3.63) is obtained.

CHAPTER 4

PARAMETER IDENTIFICATION ALGORITHM AND MULTIOBJECTIVE TOOLBOX DEVELOPMENT IN MATLAB GUI

In previous chapter, all the hyperelastic rubber models (totally ten) are presented with their material parameters. The purpose is having the best material parameters with respect to given test data. As it was stated before, Treloar data are used for uniaxial tension, equibiaxial tension and pure shear cases whereas Kawabata data are used for biaxial case to identify the parameters in this thesis. Those data sets will be given in following chapters. A method must be presented to identify the parameters with respect to given data. The aim is fitting theoretical solutions which are obtained from models with experimental measures. In other words, the aim is minimizing the error between theoretical results and experimental results. In this study, MATLAB fmincon command is used to perform this task. This command minimizes the given function according to given initial points, bounds and constraints. For this function, least square error calculation will be used. Least square error calculation is given as

$$\text{error} = \sum_{i=1}^{n} ||X_n - \bar{X}_n|| . \qquad (4.1)$$

Obtaining error as zero is the ideal case. However, this can not be obtained due to uncertainties and high nonlinearities in experimental data. Even best hyperelastic models have small errors. Thus, the aim is to have the error as small as possible for given material model.

Parameter identification process can be applied for only one deformation mode or more than one deformation modes together. However, if only one deformation mode is taken into account, identified parameters may not be suitable for other

deformation cases. Having one material parameter set is more logical because that will lead to time gain. If one material parameter set will be found, all error definitions should be added up when fmincon function is formed. However, one deformation mode can have bigger error than the other, so evaluating the error definitions equally will not lead to best minimized error for parameter identification process. Thus, weight numbers are used for each deformation mode. However, the problem is which deformation case should have the bigger weight number. Trying different weight numbers will lead to time loss. In this point, the solution is that weight numbers should be taken as unknown and they must be defined also with material parameters to have the best minimized error. In this point, constraint also must be added to fmincon command for weight numbers. Thus, summation of weight numbers is taken as 1 (one) in this study. 1 (One) will be shared between deformation modes to have the best minimized error. Error function can be written according to all the information given as

$$f = c_1 \xi_{uniaxial} + c_2 \xi_{equibiaxial} + c_3 \xi_{pureshear} . \qquad (4.2)$$

Here, c_1, c_2 and c_3 are weight numbers. $\xi_{uniaxial}$, $\xi_{equibiaxial}$ and $\xi_{pureshear}$ are the error expressions for related deformation mode written in their indices. After least square error calculation is done for related deformation mode, the expression is divided by data point number as

$$\xi = \frac{1}{n} \sum_{i=1}^{n} (P_{11} - P_{11}{}^{exp})^2 . \qquad (4.3)$$

Here P_{11} consists of the first Piola-Kirchhoff stress data points of related model, $P_{11}{}^{exp}$ consists of experimental first Piola-Kirchhoff stress data. This expression is formed for all deformation modes. Then, it is multiplied with weight function and all the expressions are added to form the error function.

The other important point is that material parameters should have the lower bound, upper bound and initial points if any information is available. For example, some

parameters can not be lower than zero according to physical laws. When all this information (error function, initial points, lower and upper bounds for all parameters, constraints) are entered to the fmincon, parameter identification can be done.

However, there is only one error calculation for biaxial case. Then, no weight number is needed for that case. Applying equation (4.3) is enough in that case to form the error function.

4.1. Matlab GUI Development for the Multiobjective Optimization Toolbox for Parameter Identification of Elastomers

All the processes from doing continuum mechanics calculations for related model to identifying the parameters and plotting the results are long and complicated processes. There are a lot of calculations to be done and a lot of points to be careful with. Thus, for minimizing the mistakes and decreasing the time loss, an user friendly interface idea also come out for this thesis. For this purpose, MATLAB GUI is one of the best options. A multiobjective optimization toolbox is developed for parameter identification of elastomers.

GUI provides the users to arrange all the information on a computer to perform the tasks easily by using various icons and menus. Push buttons, sliders, edit boxes, menus etc. and a consistent appearance will make the program easier to use. Doing all the calculations by looking a code file can lead to make mistakes. A developed GUI with a user manual will lead users to perform all the tasks faster. It also makes the users perform interactive tasks. It is also important that developed GUI should be in an understandable and predictable manner so that user should understand what to do for desired action. All the buttons should have the label for its function [30].

In GUI screen, related components can be grouped. Moreover, the results can be given with the plots on the screen. The first thing to create a GUI in MATLAB is designing the lay-out for the required tasks. Every component which is put on the

lay-out screen will have a MATLAB callback code behind. The designer should write the related codes to make the related button to perform the related tasks [30].

The multiobjective optimization toolbox for parameter identification of elastomers developed in MATLAB GUI can be seen in Figure 4.1.
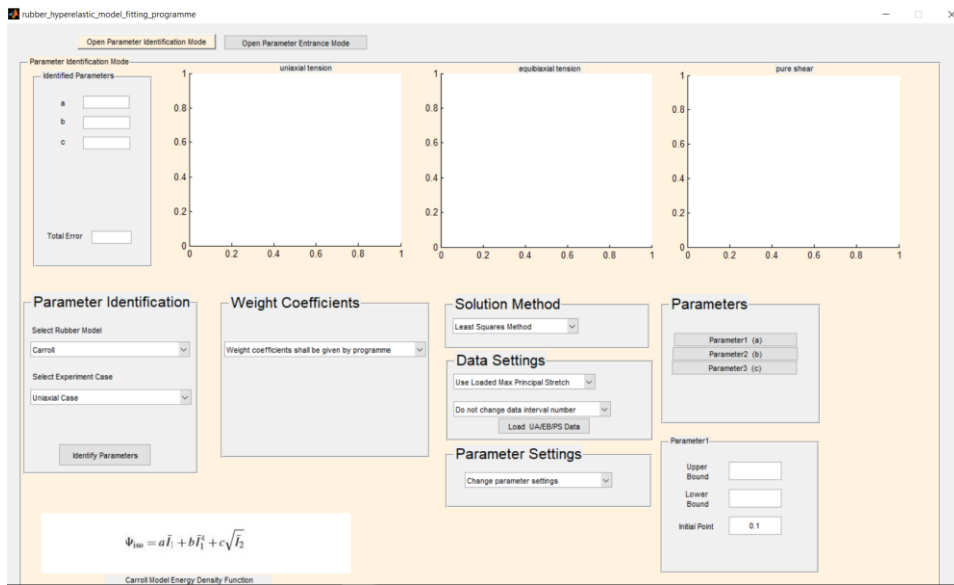

Figure 4.1: Multiobjective optimization toolbox for parameter identification of elastomers overview with parameter identification mode

As it is seen above, there are different panels on the screen. In parameter identification panel, rubber model and experimental case can be selected. As it was stated before, ten rubber material models are examined in this thesis. Thus, there are those rubber material models in the database of this toolbox. Parameter identification can be performed for only uniaxial tension case, only equibiaxial tension case, only pure shear case, equibiaxial and uniaxial tension cases together, pure shear, equibiaxial tension and uniaxial tension cases together and only biaxial case. If biaxial case is selected, biaxial data button also appears on this panel.

Weight coefficients can be identified by the program to have best minimized error. Moreover, user can enter manually. Thus, one case can be more dominant if it is desired.

There are also data settings panel. Here, stretch data can be limited until specified point. Moreover, if there are limited number of data points, these can be increased between maximum and minimum data value by using a second order polynomial. The test data for uniaxial tension, equibiaxial tension and pure shear cases are loaded from here by using "Load UA/EB/PS Data" button. After test data are loaded, the data will be plotted automatically on the plots (Figure 4.2). These plots are for Treloar data of uniaxial tension, equibiaxial tension and pure shear respectively.
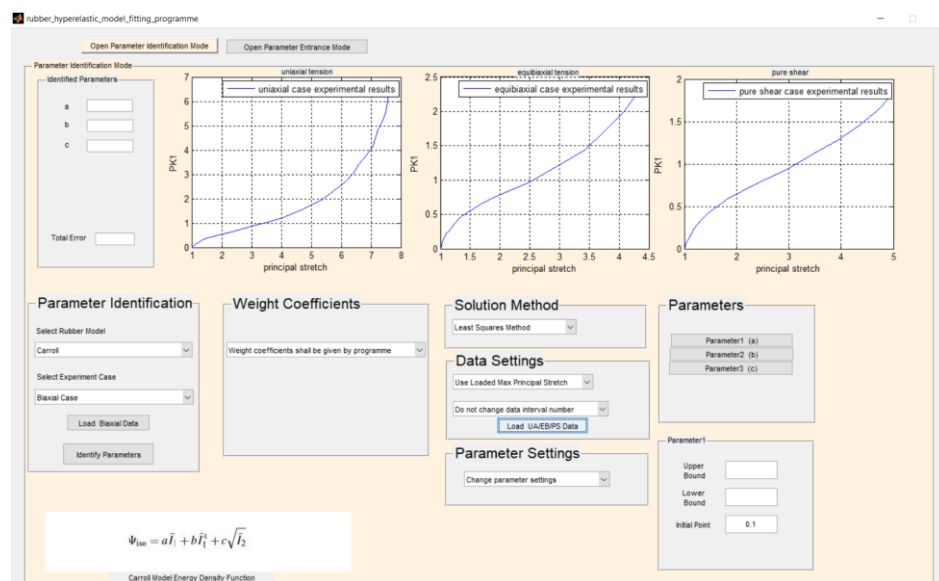
Figure 4.2: Treloar test data loaded on multiobjective optimization toolbox for parameter identification of elastomers

For biaxial case, another plot figure is opened for test data. As it was stated before, Kawabata data are used for biaxial case parameter identification process. Kawabata data can be loaded by using "Load Biaxial Data" (Figure 4.3). Another biaxial data can be entered if it is desired by adding as .mat file.
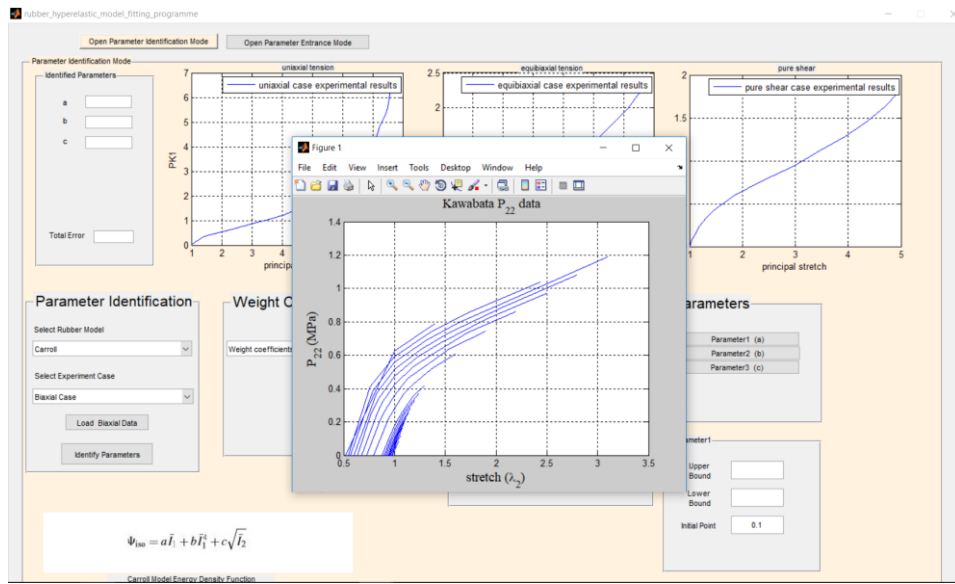
Figure 4.3: Kawabata test data loaded on multiobjective optimization toolbox for parameter identification of elastomers

In parameter settings panel, parameters can be entered manually or implemented settings in the program can be used. If user would like to change parameter settings, they (upper and lower bound, initial point) can be changed for each parameter by selecting related parameter on the parameters panel.

After all necessary selections are done, parameter identification process can be initiated by using "Identify Parameters" button. Then, the results will be plotted on the test data. Moreover, on the identified parameters panel, results can be seen. Total error can also be seen from here. Total error gives an idea for the quality of parameter identification. Moreover, it can be seen from plots how good parameter identification is visually. The results on the toolbox for Carroll model are shown below for Treloar data and Kawabata data (Figure 4.4, Figure 4.5). This process is applied for all the models and detailed results and plots will be given in the next chapter. For Treloar data, parameters will be identified for three cases together. As it was stated before, parameters can be found for each case if it is desired. The results are given for first Piola-Kirchhoff stress.
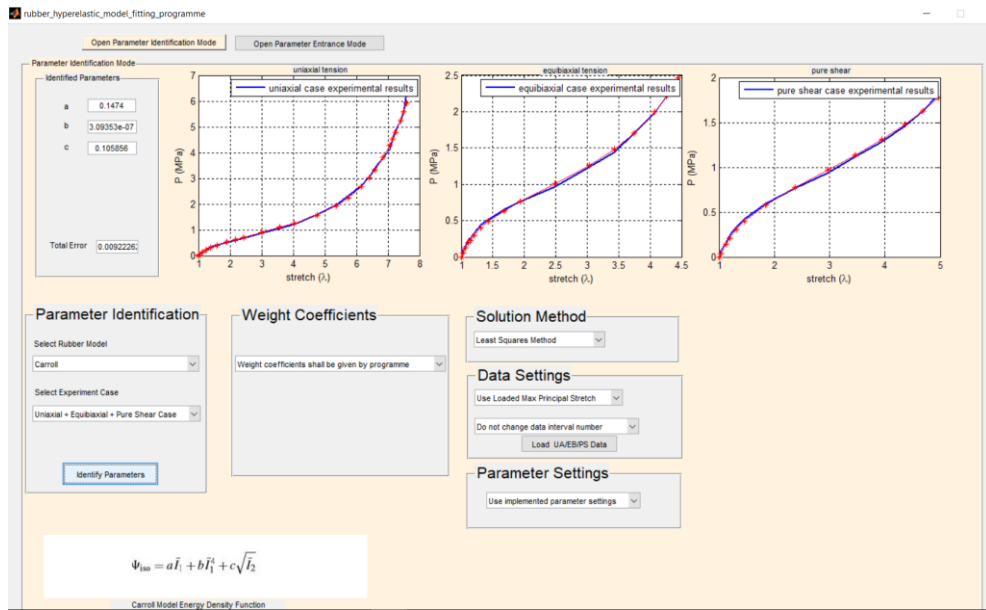
Figure 4.4: The results given on multiobjective optimization toolbox for parameter identification of elastomers for Carroll model example by using Treloar data
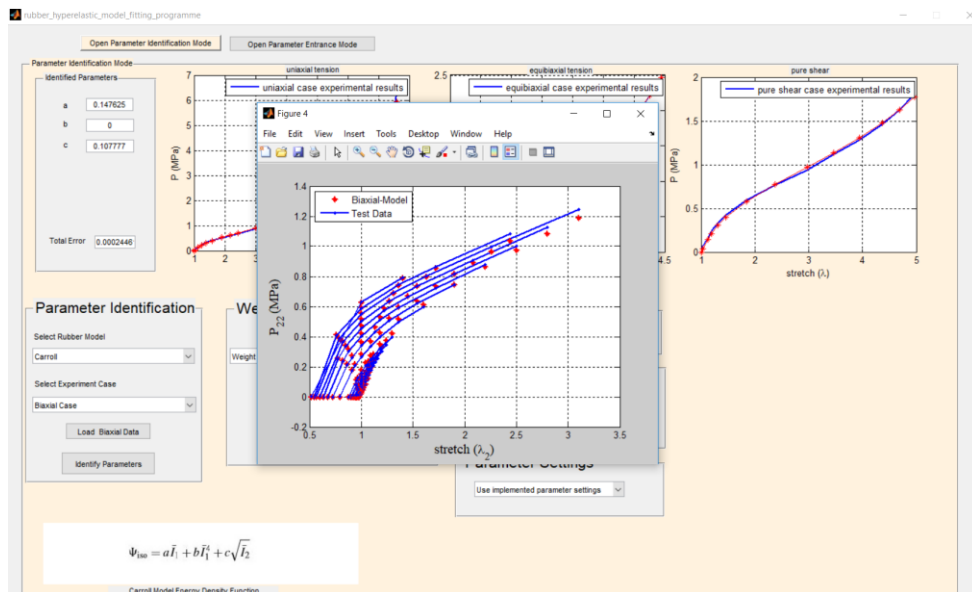

Figure 4.5: The results given on multiobjective optimization toolbox for parameter identification of elastomers for Carroll model example by using Kawabata data

There is also another mode of the toolbox except parameter identification mode. If one has the identified parameters, those parameters can be entered to the toolbox. Toolbox can take those parameters and plot the results with test data stretches and compare the results on plots by using desired model (Figure 4.5).
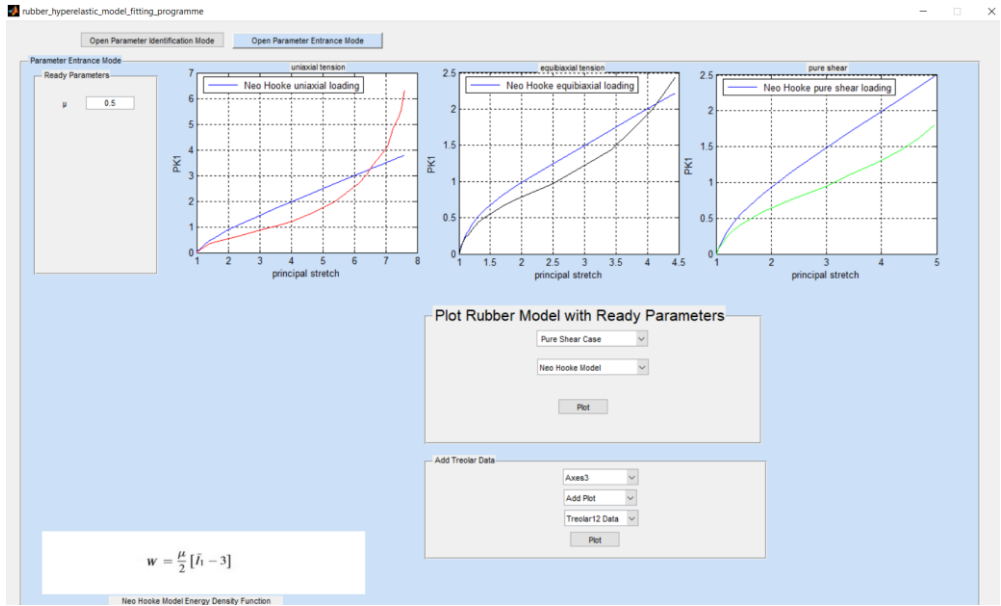
Figure 4.6: Multiobjective optimization toolbox for parameter identification of elastomers overview with parameter entrance mode

So, any Treloar data can be plotted and it can be compared with the desired rubber material model with the ready parameters which is obtained from some sources.

As it was stated before, GUI provides the users to have an interactive environment and time gain.

CHAPTER 5

PARAMETER IDENTIFICATION RESULTS OF ELASTOMER MODELS

Necessary continuum mechanics calculations which was given in Chapter 2 and Chapter 3 are done and then parameter identification process is applied for each model by using the toolbox which was given in Chapter 4. The corresponding identified parameters and errors of each model for uniaxial tension, equibiaxial tension and pure shear cases with respect to Treloar data are given in Table 5.1.

Table 5.1: Identified parameters of elastomer models by using Treloar data

Model Name Identified Parameters, Error	Model Name Identified Parameters, Error
	Ogden Model μ_1=1.718, μ_2=6.969, μ_3=-2.064, α_1=0.428, α_2=0.0000223, α_3= -0.00933, Error=0.132
Neo-Hooke Model μ=0.489, Error=0.980	
	Shariff Model E=1.122, α_0=0.915, α_1=0.0369, α_2=0.0000786, α_3=0.0244, Error=0.0075
Mooney Model C_1=0.23, C_2=0.0001, Error=1.056	
Biderman Model C_{10}=0.184, C_{01}=0.0028, C_{20}= - 0.00176, C_{30}= 0.0000442, Error=0.169	Eight-Chain Model μ=0.287, N=26.478, Error=0.0445
Yeoh Model C_1=0.177, C_2=-0.0012, C_3= 0.0000377, Error=0.051	Extended Tube Model G_c=0.195, δ=0.0954, β=0.129, G_e=0.199, Error=0.0073
Carroll Model a=0.147, b=3.093 x 10^{-7}, c=0.106, Error=0.0092	Microsphere Model μ=0.293, N=22.029, p=1.469, U=0.744, q=0.106, Error=0.004

The corresponding weight coefficients of deformation modes for each model with uniaxial tension, equibiaxial tension and pure shear cases together with respect to Treloar data are given in Table 5.2.

Table 5.2: Identified weight coefficients of elastomer models by using Treloar data

Model Name Weight Coefficients	Model Name Weight Coefficients
Neo-Hooke Model $c_1 = 0.1$, $c_2 = 0.8$, $c_3 = 0.1$	Ogden Model $c_1 = 0.33$, $c_2 = 0.33$, $c_3 = 0.33$
Mooney Model $c_1 = 0.59$, $c_2 = 0.21$, $c_3 = 0.2$	Shariff Model $c_1 = 0.2$, $c_2 = 0.6$, $c_3 = 0.2$
Biderman Model $c_1 = 0.53$, $c_2 = 0.2$, $c_3 = 0.27$	Eight-Chain Model $c_1 = 0.6$, $c_2 = 0.2$, $c_3 = 0.2$
Yeoh Model $c_1 = 0.8$, $c_2 = 0.1$, $c_3 = 0.1$	Extended Tube Model $c_1 = 0.6$, $c_2 = 0.2$, $c_3 = 0.2$
Carroll Model $c_1 = 0.8$, $c_2 = 0.1$, $c_3 = 0.1$	Microsphere Model $c_1 = 0.41$, $c_2 = 0.39$, $c_3 = 0.2$

As it was stated before, c_1 is weight coefficient of uniaxial case, c_2 is weight coefficient of equibiaxial case and c_3 is weight coefficient of pure shear case. Sum of weight coefficients is 1 (one).

The corresponding identified parameters and errors of each model for biaxial case with respect to Kawabata data are given in Table 5.3. Since there is only experimental case (biaxial tension), there is not any weight coefficient to be calculated.

Table 5.3: Identified parameters of elastomer models by using Kawabata data

Model Name Identified Parameters, Error	Model Name Identified Parameters, Error
Neo-Hooke Model μ=0.448, Error=0.00396	Ogden Model μ_1=1.198, μ_2=5.997, μ_3=-2.420, α_1=0.66, α_2=0.000346, α_3= -0.00403, Error=0.0000948
Mooney Model C_1=0.199, C_2=0.00349, Error=0.00352	Shariff Model E=1.09, α_0=0.809, α_1=0.0531, α_2=0, α_3=0.0289, Error=0.000125
Biderman Model C_{10}=0.191, C_{01}=0.0190, C_{20}= - 0.00653, C_{30}= 0.0000231, Error=0.000665	Eight-Chain Model μ=0.4, N=26.478, Error=0.00482
Yeoh Model C_1=0.209, C_2=0.00384, C_3= 0.000176, Error=0.00339	Extended Tube Model G_c=0.256, δ=0.0572, β=0.126, G_e=0.159, Error=0.0000289
Carroll Model a=0.148, b=0, c=0.107, Error=0.000244	Microsphere Model μ=0.304, N=22.010, p=1.475, U=0.741, q=0.0834, Error=0.0001276

The toolbox is designed to select the best elastomer model from a given set of experiments. Certain criteria should be determined to compare hyperelastic constitutive models of elastomers. As it was stated before, a hyperelastic constitutive model should reproduce 'S' shaped response of rubbers, not to have problem with different deformation modes, have parameters as few as possible and have a simple mathematical formulation. First and second criteria can be examined by comparing the errors. Third and fourth criteria will provide time gain for calculations. Performance of those models are compared by using Treloar's data and Kawabata's data separately.

5.1. Performance of Hyperelastic Models on Treloar's Data

In algorithm, having the smallest error for three deformation modes with one material set is aimed for parameter identification of elastomer models by using Treloar's data. Obtaining better fit quality requires a smaller error. That means 'S' shaped response can also be obtained better. According to Table 5.1, microsphere model has the smallest error between ten hyperelastic constitutive models. Moreover, Shariff, extended tube and Carroll models have also good results. Thus, those four models (two phenomenological models and two micro-mechanical models) meet the requirements for first and second criteria. Neo-Hooke and Mooney models have the worst fit quality.

Having fewer material parameters was also another criterion. In this point, four elastomer models which have the smallest errors can be compared. Carroll model have the least material parameters which is 3 (three). However, microsphere and extended tube models have four and Shariff model has five material parameters. Moreover, Carroll model has the simplest mathematical model among those four elastomer models. However, extended tube and microsphere model relate macroscopic mechanical behavior to physical structure at molecular level.

The plots are given for uniaxial tension, equibiaxial tension and pure shear cases for related hyperelastic model by comparing related Treloar's data. The results are discussed for each model. The first Piola-Kirchhoff stress is used in Treloar's data.

Those results give information for selecting the right hyperelastic model for a particular application. Because, some hyperelastic models perform well in all region of deformations. Low stretch, moderate stretch and large stretch can be defined as $1 < \lambda < \frac{1}{3}\lambda_{max}$, $1 < \lambda < \frac{2}{3}\lambda_{max}$ and $1 < \lambda < \lambda_{max}$ respectively. Some hyperelastic models can give good results on a specific region. Thus, if a particular application contains only low stretch region, a simpler model which give good results on this region can be used.
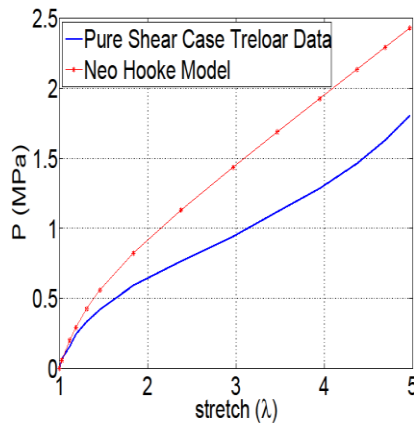
5.1.1. Neo-Hooke Model Results

The performance of Neo-Hooke model on Treloar's data is given in Figure 5.1 according to identified parameters in Table 5.1. S shape can not be obtained due to simple model structure. In low stretch region, reasonable results are obtained.
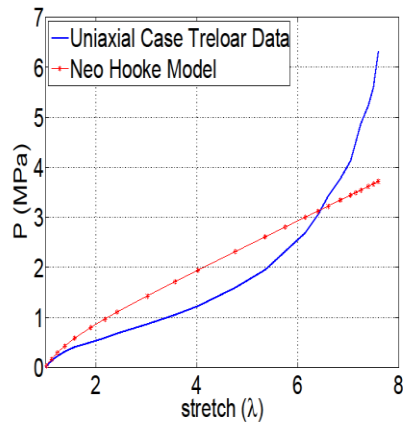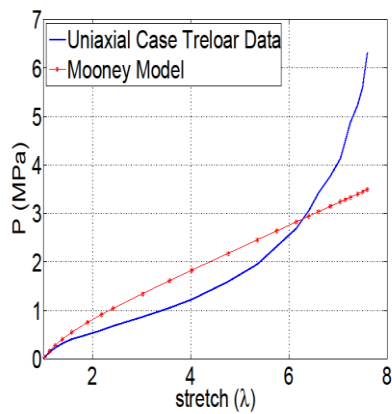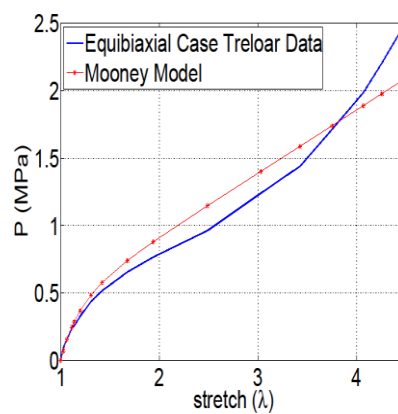

(a)
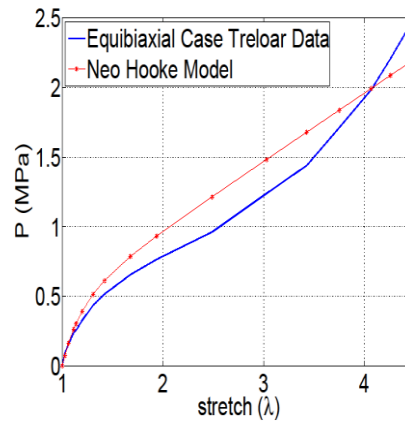
(b)

(c)

Figure 5.1: Performance of Neo-Hooke model on Treloar's data for first Piola-Kirchhoff stress: (a) Uniaxial Tension (b) Equibiaxial Tension (c) Pure Shear
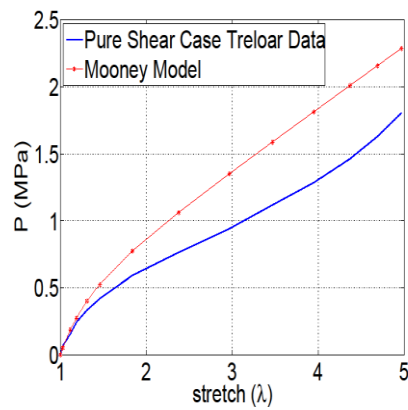
5.1.2. Mooney Model Results

The performance of Mooney model on Treloar's data is given in Figure 5.2 according to identified parameters in Table 5.1. S shape can not be obtained due to not having complex model structure like Neo-Hooke model. Thus, only in low stretch region reasonable results are obtained.

(a)   (b)

(c)

Figure 5.2: Performance of Mooney model on Treloar's data for first Piola-Kirchhoff stress: (a) Uniaxial Tension (b) Equibiaxial Tension (c) Pure Shear

5.1.3. Biderman Model Results

The performance of Biderman model on Treloar's data is given in Figure 5.3 according to identified parameters in Table 5.1. There are better models than Biderman however this model provides acceptable results. This model structure can produce S shape. It fits uniaxial case slightly better than other cases.
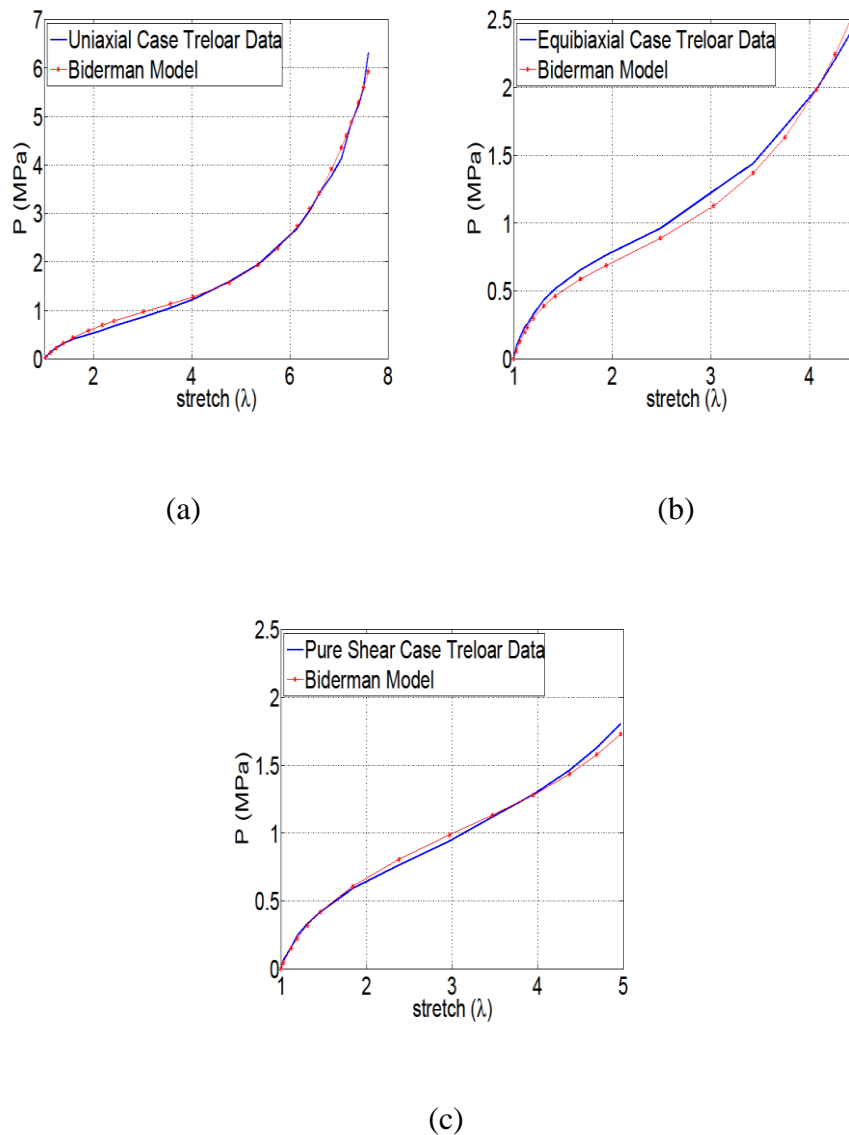

(a)   (b)

(c)

Figure 5.3: Performance of Biderman model on Treloar's data for first Piola-Kirchhoff stress: (a) Uniaxial Tension (b) Equibiaxial Tension (c) Pure Shear

5.1.4. Yeoh Model Results

The performance of Yeoh model on Treloar's data is given in Figure 5.4 according to identified parameters in Table 5.1. This model structure can produce S shape. However, equibiaxial case results shall not be enough for specific applications in moderate and large stretches.
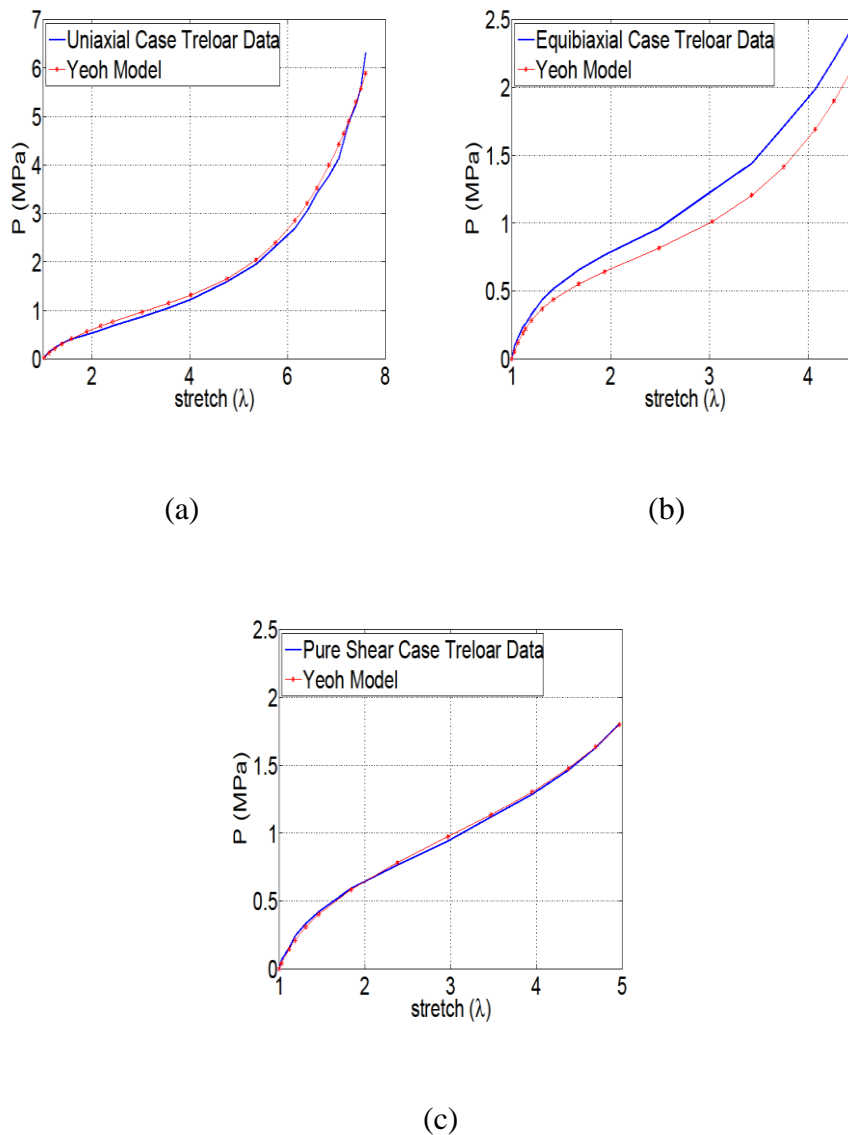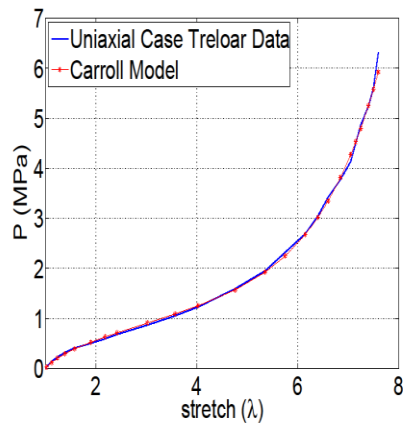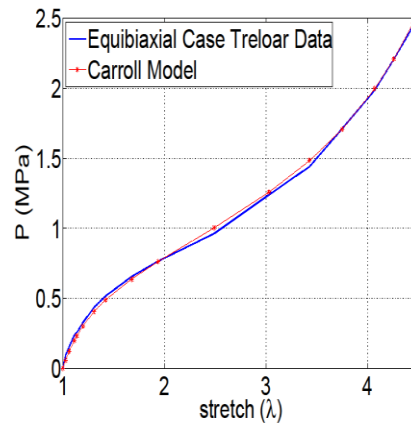

(a)

(b)

(c)

Figure 5.4: Performance of Yeoh model on Treloar's data for first Piola-Kirchhoff stress: (a) Uniaxial Tension (b) Equibiaxial Tension (c) Pure Shear
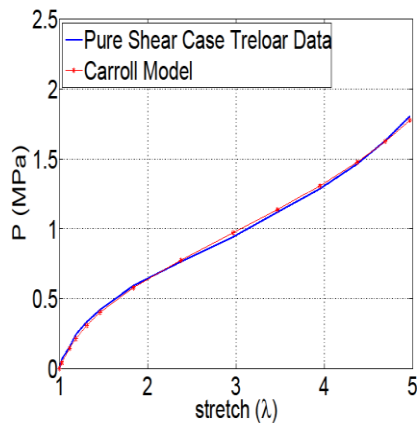
5.1.5. Carroll Model Results

The performance of Carroll model on Treloar's data is given in Figure 5.5 according to identified parameters in Table 5.1. This model structure can produce S shape perfectly. Carroll model shows remarkable performance. Only in moderate stretches of equibiaxial tension, performance could be better.

(a)   (b)

(c)

Figure 5.5: Performance of Carroll model on Treloar's data for first Piola-Kirchhoff stress: (a) Uniaxial Tension (b) Equibiaxial Tension (c) Pure Shear

5.1.6. Shariff Model Results

The performance of Shariff model on Treloar's data is given in Figure 5.6 according to identified parameters in Table 5.1. This model structure can produce S shape perfectly and shows remarkable performance like Carroll model. Only in stretch interval of 2<λ<3 in equibiaxial tension, performance could be better.
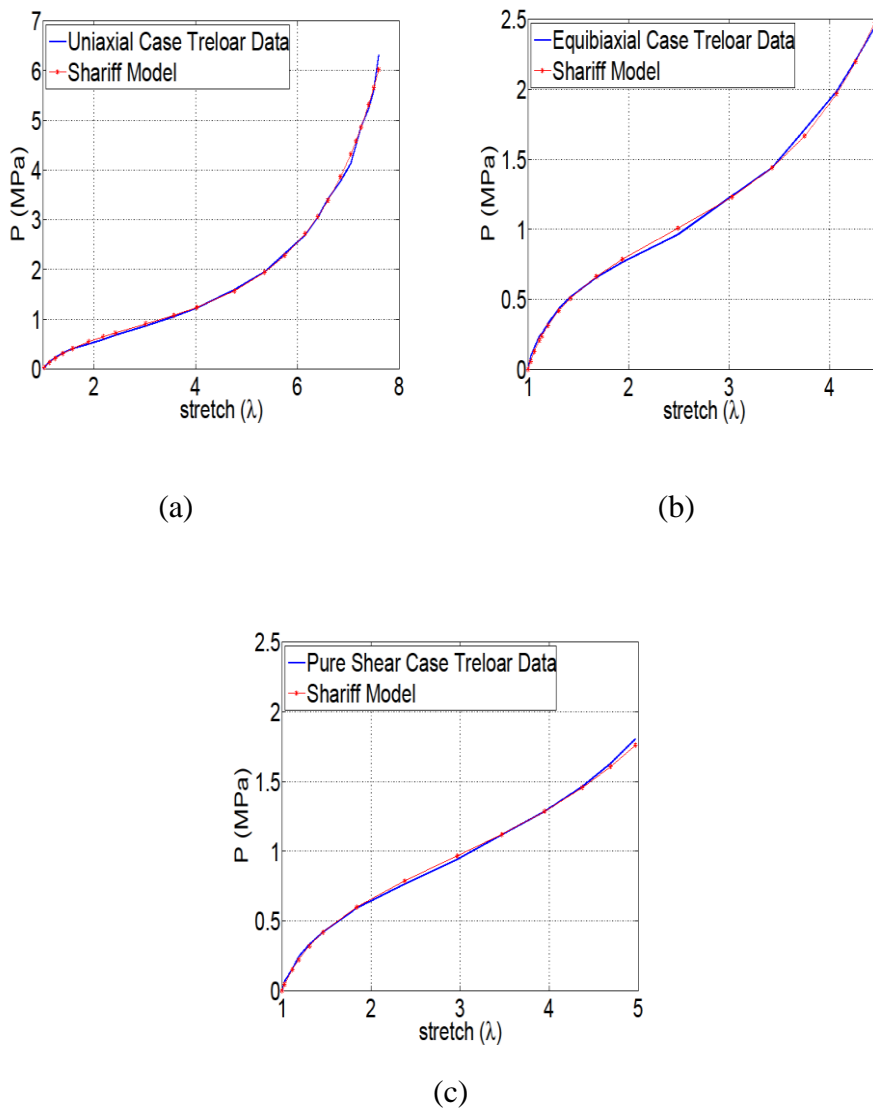
(a)

(b)

(c)

Figure 5.6: Performance of Shariff model on Treloar's data for first Piola-Kirchhoff stress: (a) Uniaxial Tension (b) Equibiaxial Tension (c) Pure Shear

5.1.7. Ogden Model Results

The performance of Ogden model on Treloar's data is given in Figure 5.7 according to identified parameters in Table 5.1. This model structure can produce S shape and shows good performance. Only equibiaxial tension performance could be better in moderate and large stretch regions.
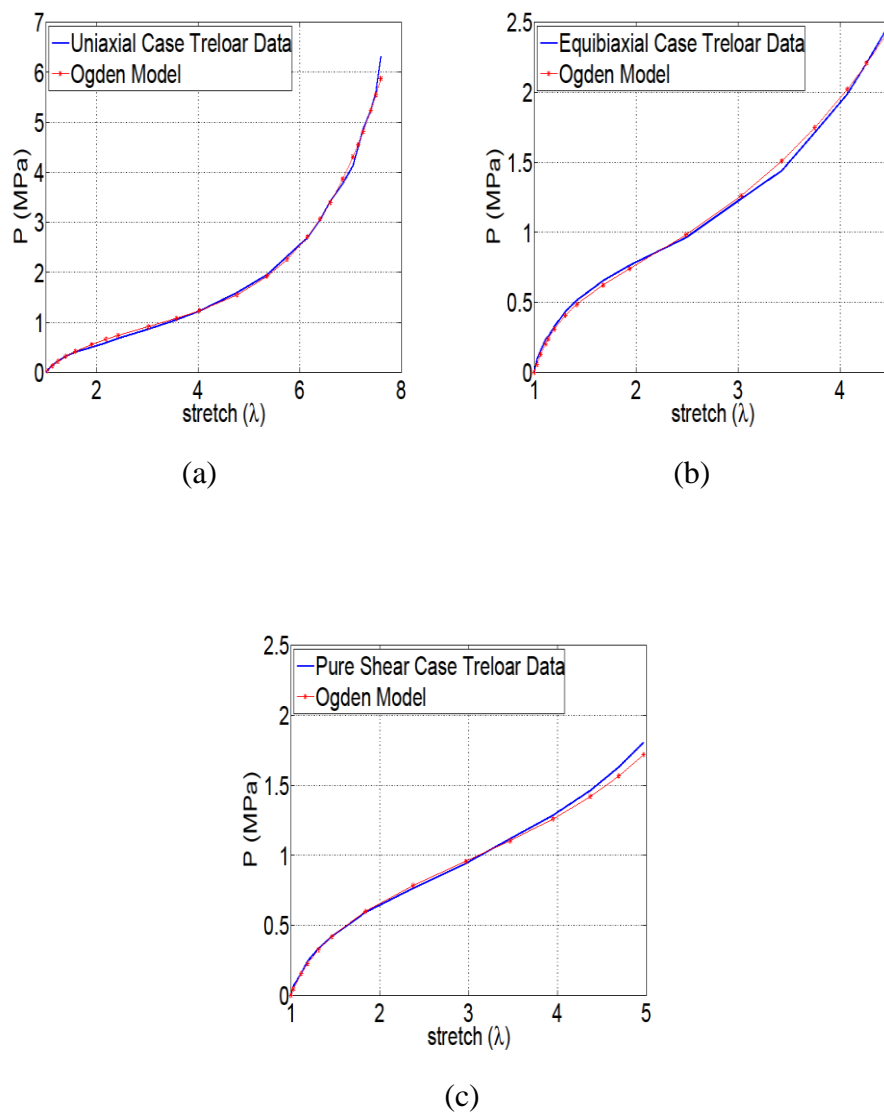

(a)

(b)

(c)

Figure 5.7: Performance of Ogden model on Treloar's data for first Piola-Kirchhoff stress: (a) Uniaxial Tension (b) Equibiaxial Tension (c) Pure Shear

5.1.8. Eight-Chain Model Results

The performance of eight-chain model on Treloar's data is given in Figure 5.8 according to identified parameters in Table 5.1. This model structure does not produce S shape perfectly. Thus, the performance is not satisfying for equibiaxial and pure shear cases. However, it is better than Neo-Hooke and Mooney Models in any case.
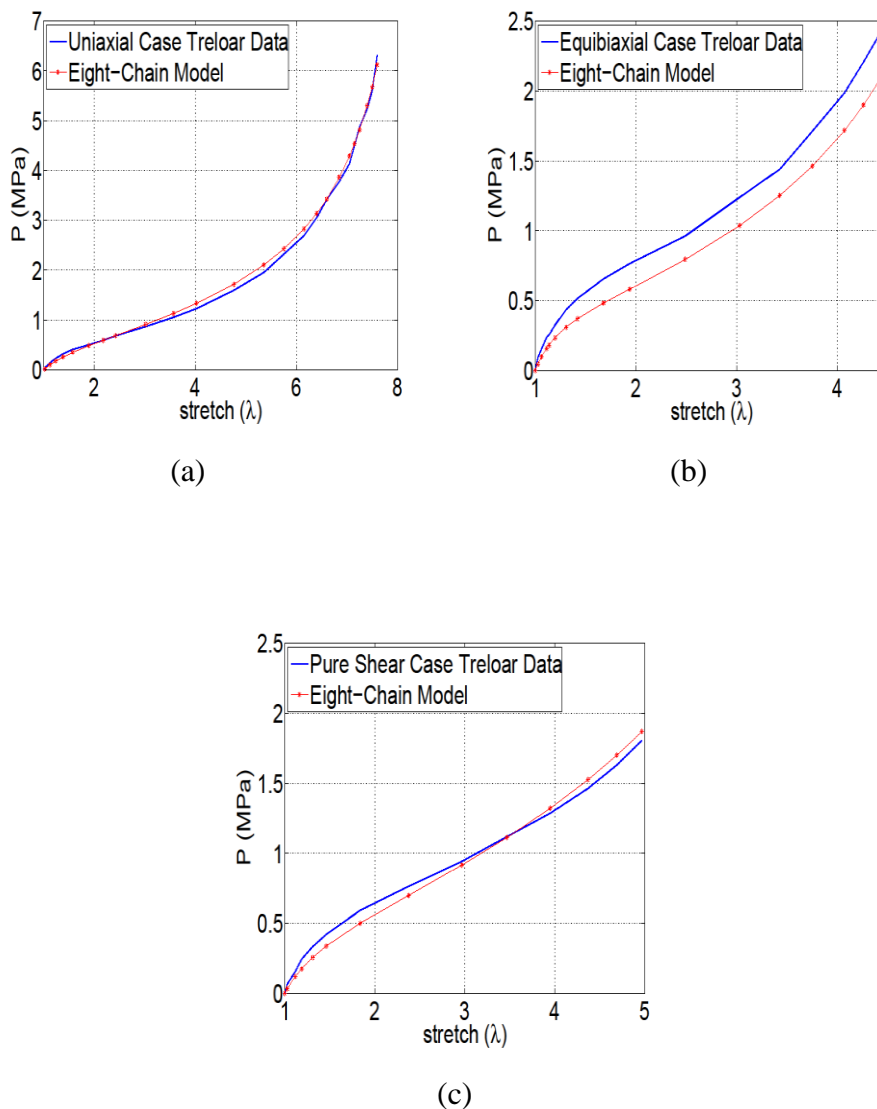

(a)

(b)

(c)

Figure 5.8: Performance of eight-chain model on Treloar's data for first Piola-Kirchhoff stress: (a) Uniaxial Tension (b) Equibiaxial Tension (c) Pure Shear

5.1.9. Extended Tube Model Results

The performance of extended tube model on Treloar's data is given in Figure 5.9 according to identified parameters in Table 5.1. This model structure can produce S shape and shows remarkable performance. Only equibiaxial tension performance could be better in moderate and large stretch regions.
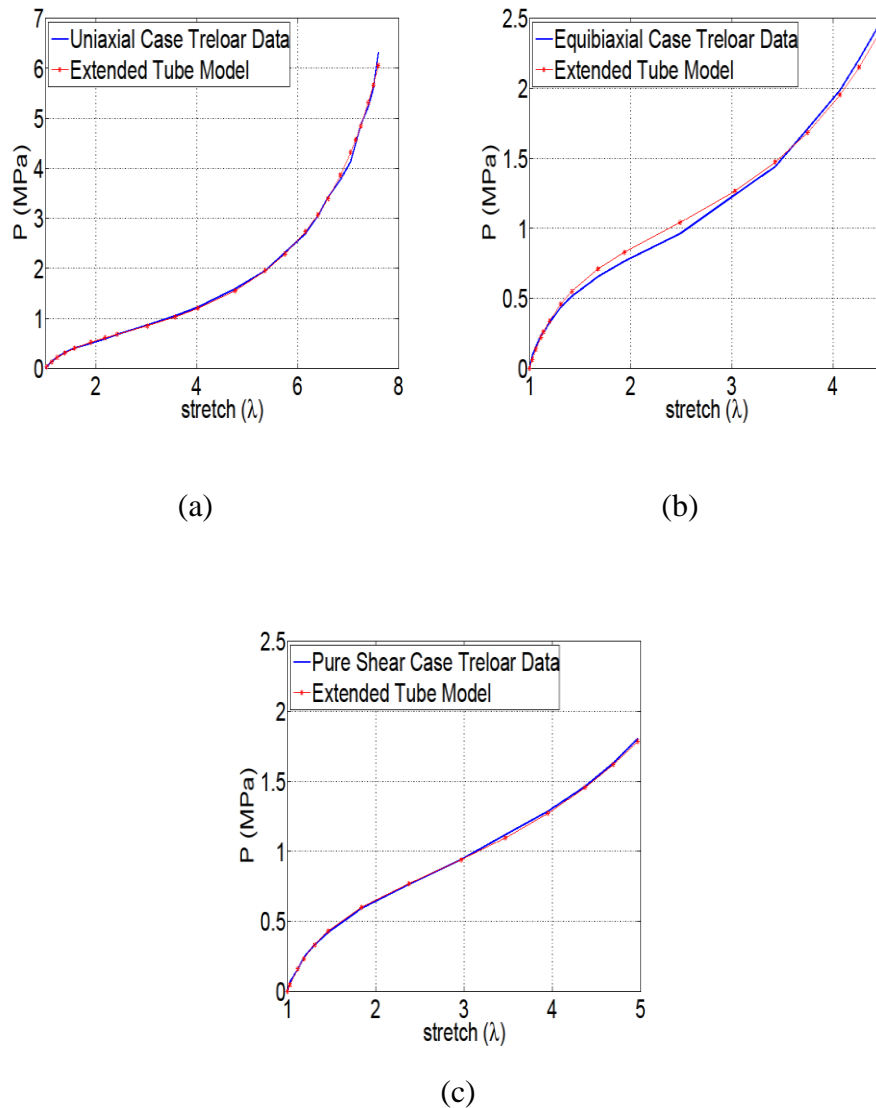

(a)

(b)

(c)

Figure 5.9: Performance of extended tube model on Treloar's data for first Piola-Kirchhoff stress: (a) Uniaxial Tension (b) Equibiaxial Tension (c) Pure Shear

5.1.10. Microsphere Model Results

The performance of microsphere model on Treloar's data is given in Figure 5.10 according to identified parameters in Table 5.1. This model structure can produce S shape perfectly. Microsphere model shows remarkable performance.
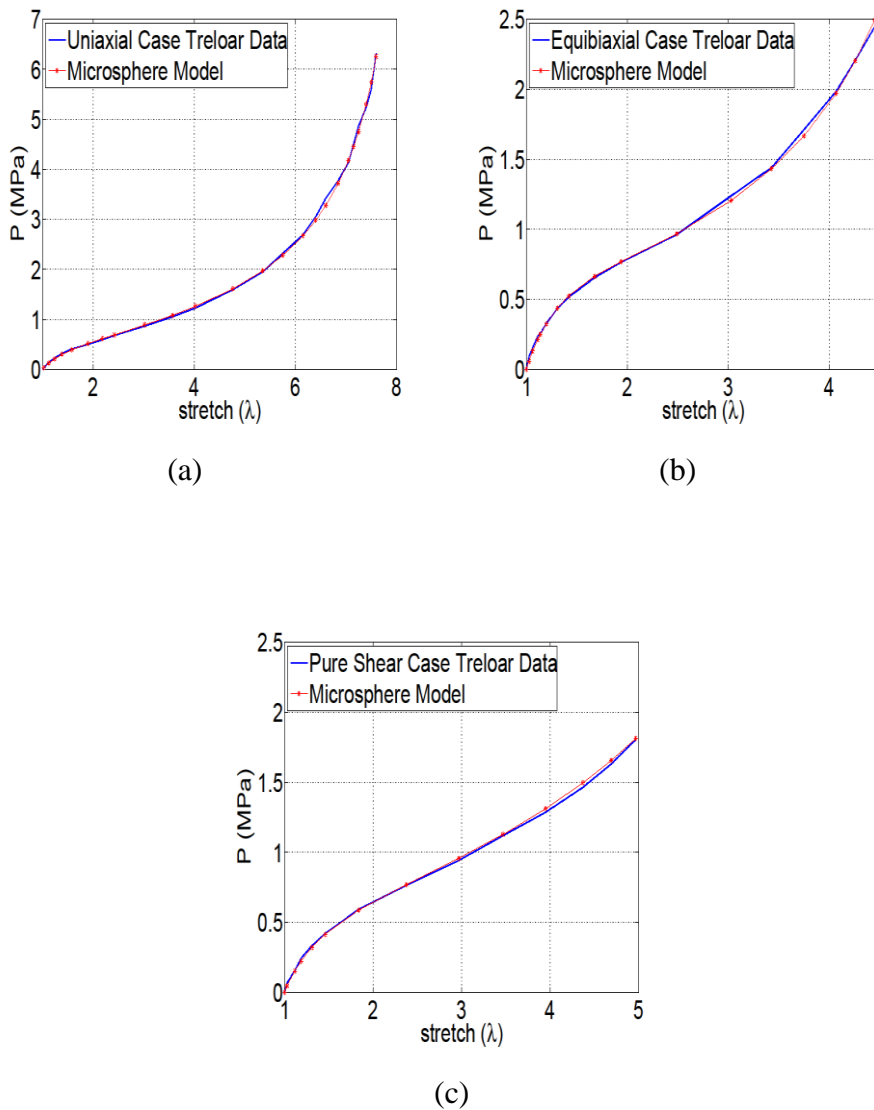

(a)

(b)

(c)

Figure 5.10: Performance of microsphere model on Treloar's data for first Piola-Kirchhoff stress: (a) Uniaxial Tension (b) Equibiaxial Tension (c) Pure Shear

5.2. Performance of Hyperelastic Models on Kawabata's Data

Treloar's data consist of three deformation cases. Thus, algorithm aims to have the smallest error for three cases together. However, biaxial case is examined separately from uniaxial tension, equibiaxial tension and pure shear because another data, called Kawabata data, are used for parameter identification algorithm. Examining biaxial case with other deformation cases would decrease the fit quality of other deformation cases.

Many researchers have used planar biaxial tension to determine the general form of the strain energy functions of elastomers [31]. In biaxial case, two different stresses occur in those two directions. In this thesis, P_{22} of Kawabata data are used for parameter identification algorithm (Figure 5.11).
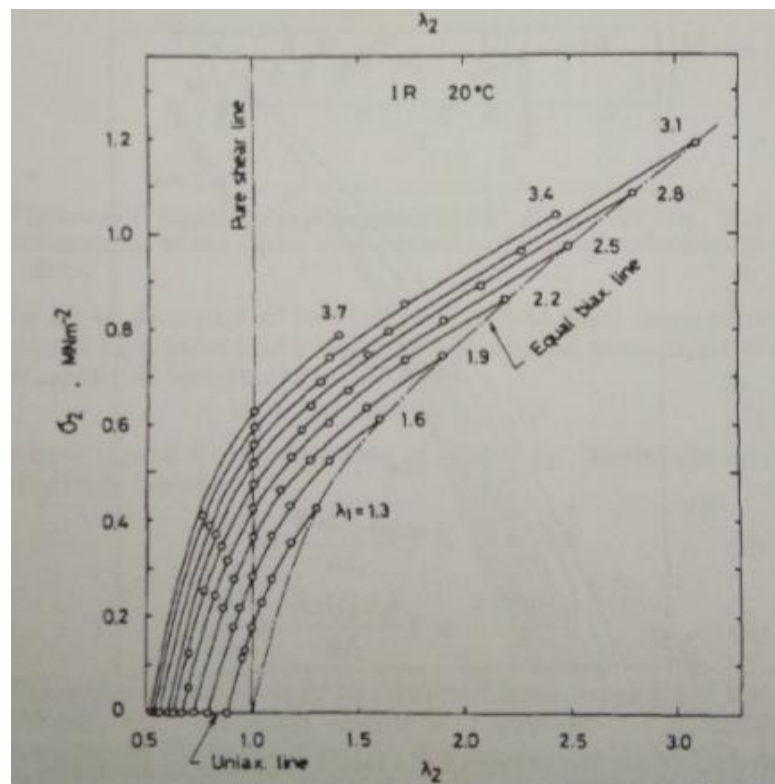

Figure 5.11: Stress P_{22} as function of the principal ratios of λ_1 and λ_2 [5]

Since there is only 1 (one) case, weight coefficients are not needed for parameter identification process. Kawabata data contain uniaxial tension, equibiaxial tension and pure shear lines in itself.

According to Table 5.3, extended tube model has the smallest error among ten elastomer models for parameter identification by using Kawabata data. Ogden model has the second smallest error on Kawabata data. Between those two models, extended tube model has the fewer material parameters. Thus, extended tube model seems as the best model for parameter identification by using Kawabata data. Moreover, extended tube model relates macroscopic mechanical behavior to physical structure at molecular level.

The plots are given for biaxial tension case for related hyperelastic model with Kawabata data. The results are discussed for each model.

5.2.1. Neo-Hooke Model Results

The performance of Neo-Hooke model on Kawabata data is given in Figure 5.12 according to identified parameters in Table 5.3. As it is seen from the plot, Neo-Hooke model performance on Kawabata data is not satisfying due to insufficient model structure.
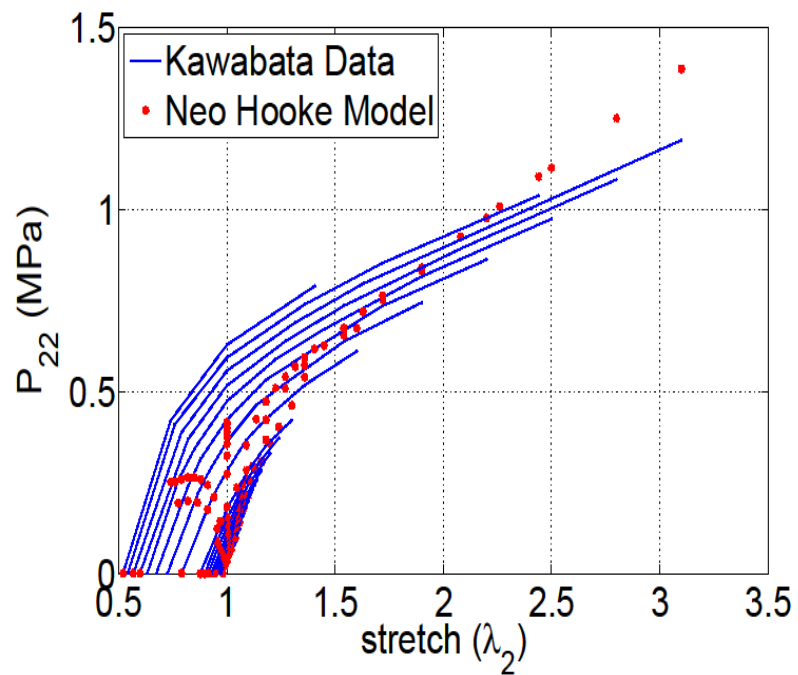

Figure 5.12: Performance of Neo-Hooke model on Kawabata's data for first Piola-Kirchhoff stress P_{22}

5.2.2. Mooney Model Results

The performance of Mooney model on Kawabata data is given in Figure 5.13 according to identified parameters in Table 5.3. As it is seen from the plot, Mooney model performance on Kawabata data is not satisfying due to insufficient model structure like Neo-Hooke model.
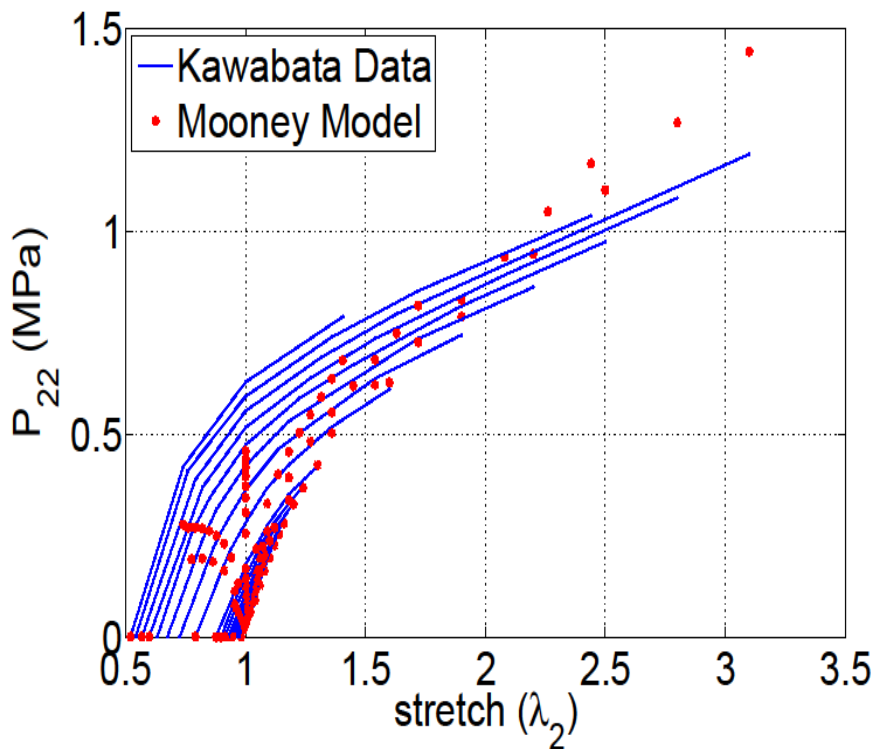

Figure 5.13: Performance of Mooney model on Kawabata's data for first Piola-Kirchhoff stress P_{22}

5.2.3. Biderman Model Results

The performance of Biderman model on Kawabata data is given in Figure 5.14 according to identified parameters in Table 5.3. As it is seen from the plot, Biderman model performance on Kawabata data is perfect in low stretch region of λ_2.
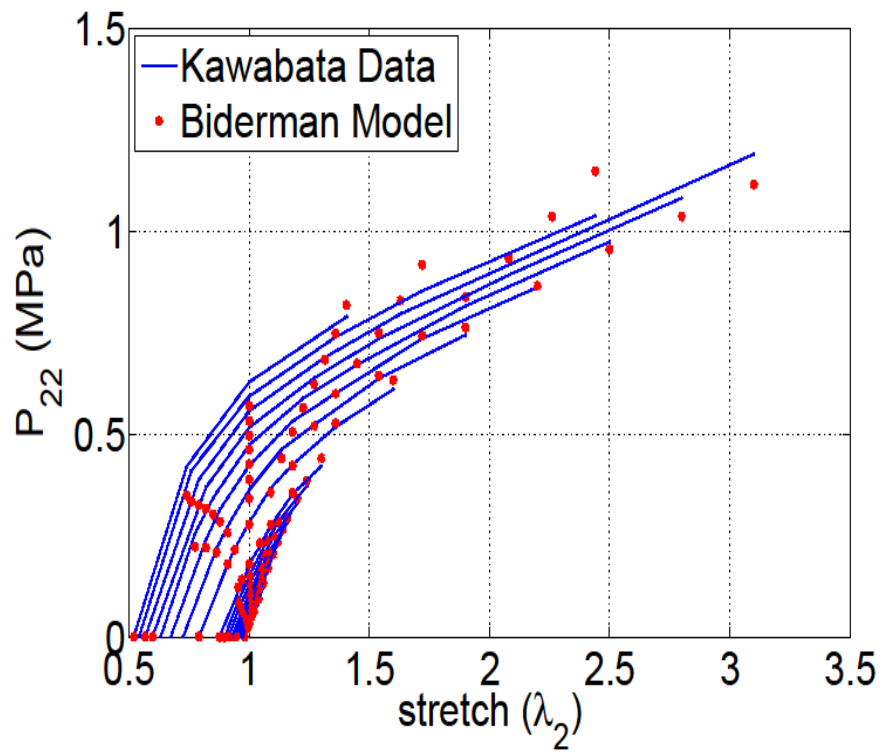

Figure 5.14: Performance of Biderman model on Kawabata's data for first Piola-Kirchhoff stress $\mathbf{P_{22}}$

5.2.4. Yeoh Model Results

The performance of Yeoh model on Kawabata data is given in Figure 5.15 according to identified parameters in Table 5.3. As it is seen from the plot, Yeoh model performance on Kawabata data is not satisfying. Yeoh model has good performance on uniaxial and equibiaxial case of Treloar data. However, it does not perform well on Kawabata data.
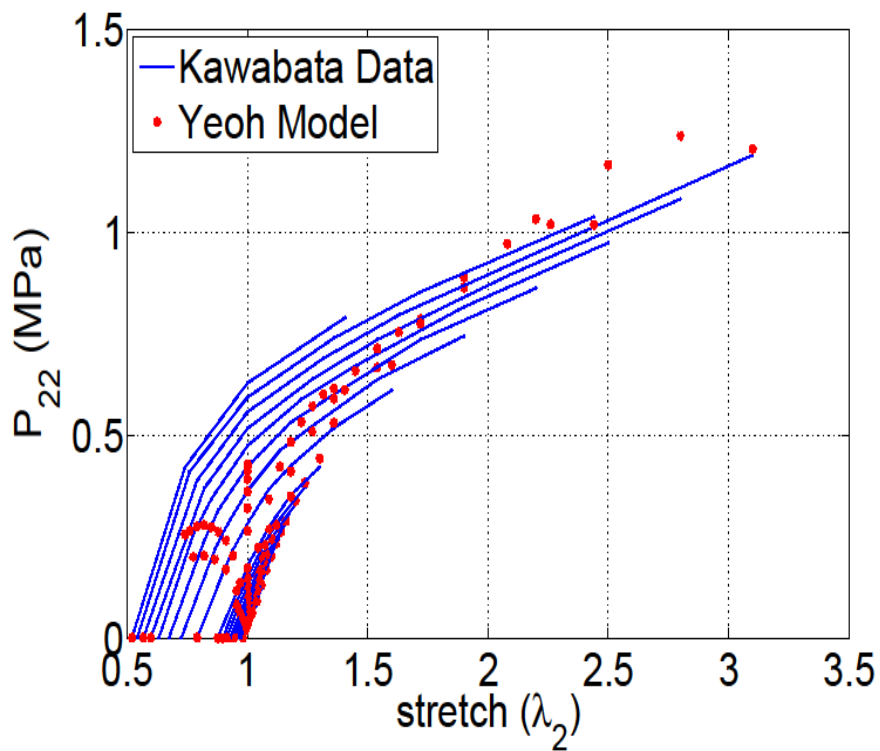

Figure 5.15: Performance of Yeoh model on Kawabata's data for first Piola-Kirchhoff stress P_{22}

5.2.5. Carroll Model Results

The performance of Carroll model on Kawabata data is given in Figure 5.16 according to identified parameters in Table 5.3. As it is seen from the plot, Carroll model performance on Kawabata data is remarkable. Only in large deformation region of λ_2, the error is increasing compared to the other deformation regions.

Figure 5.16: Performance of Carroll model on Kawabata's data for first Piola-Kirchhoff stress $\mathbf{P_{22}}$

5.2.6. Shariff Model Results

The performance of Shariff model on Kawabata data is given in Figure 5.17 according to identified parameters in Table 5.3. As it is seen from the plot, Shariff model performance on Kawabata data is remarkable on all deformation regions of λ_2.
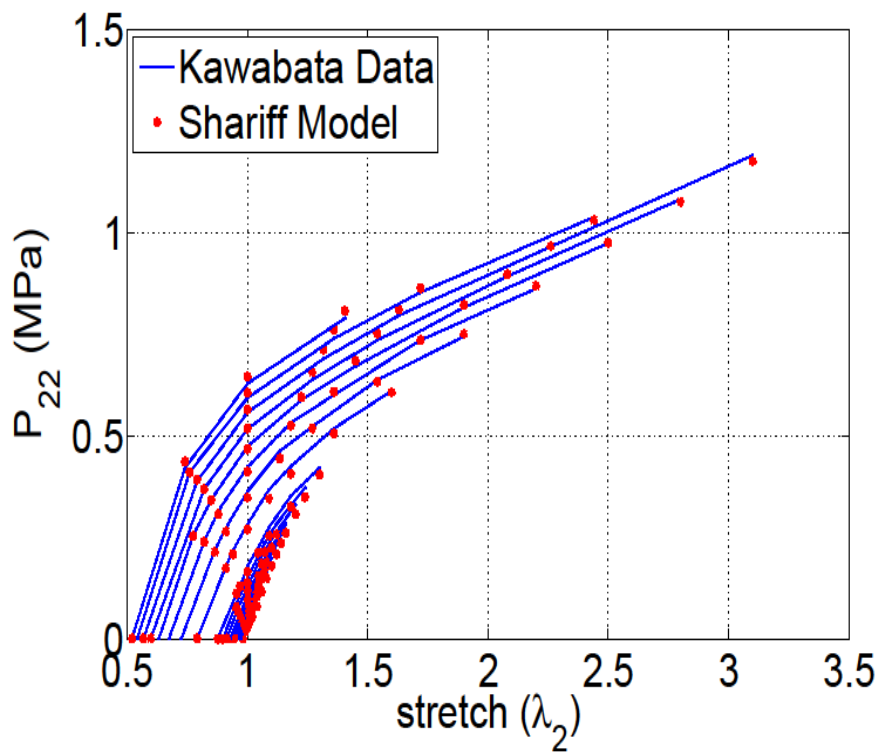
Figure 5.17: Performance of Shariff model on Kawabata's data for first Piola-Kirchhoff stress $\mathbf{P_{22}}$

5.2.7. Ogden Model Results

The performance of Ogden model on Kawabata data is given in Figure 5.18 according to identified parameters in Table 5.3. As it is seen from the plot, Ogden model performance on Kawabata data is remarkable. Only in large deformation region of λ_2, the error is increasing compared to the other deformation regions.
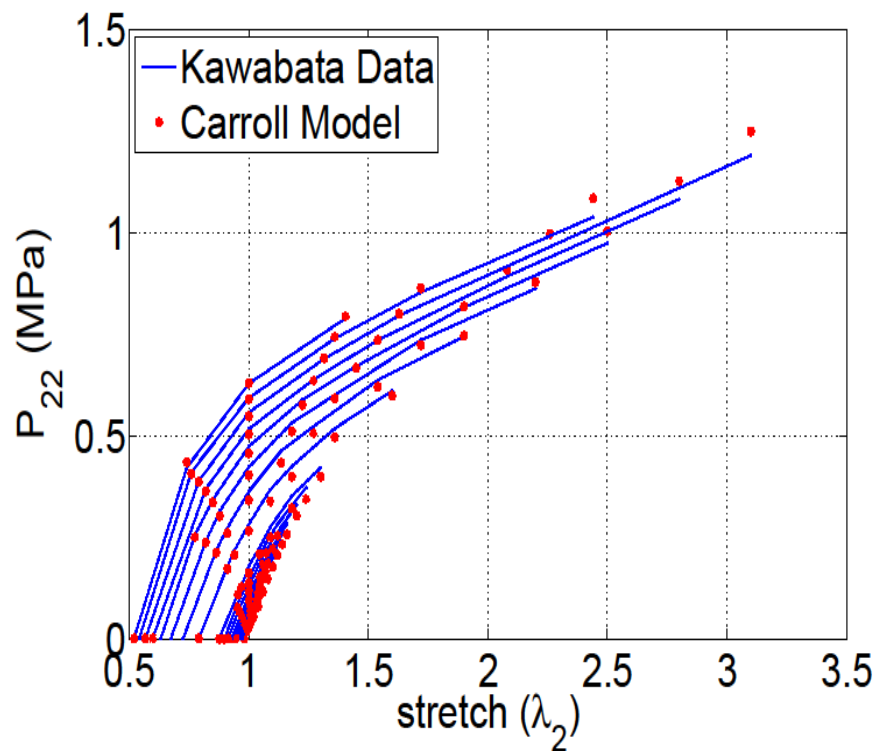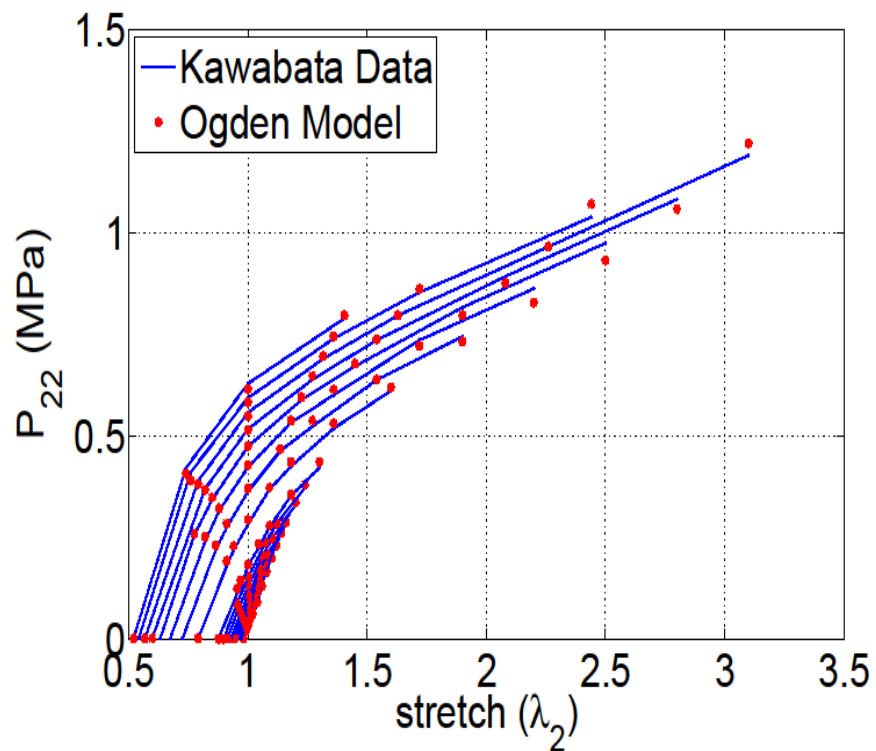

Figure 5.18: Performance of Ogden model on Kawabata's data for first Piola-Kirchhoff stress $\mathbf{P_{22}}$

5.2.8. Eight-Chain Model Results

The performance of eight-chain model on Kawabata data is given in Figure 5.19 according to identified parameters in Table 5.3. As it is seen from the plot, eight-chain model performance on Kawabata data is not satisfying due to insufficient model structure.
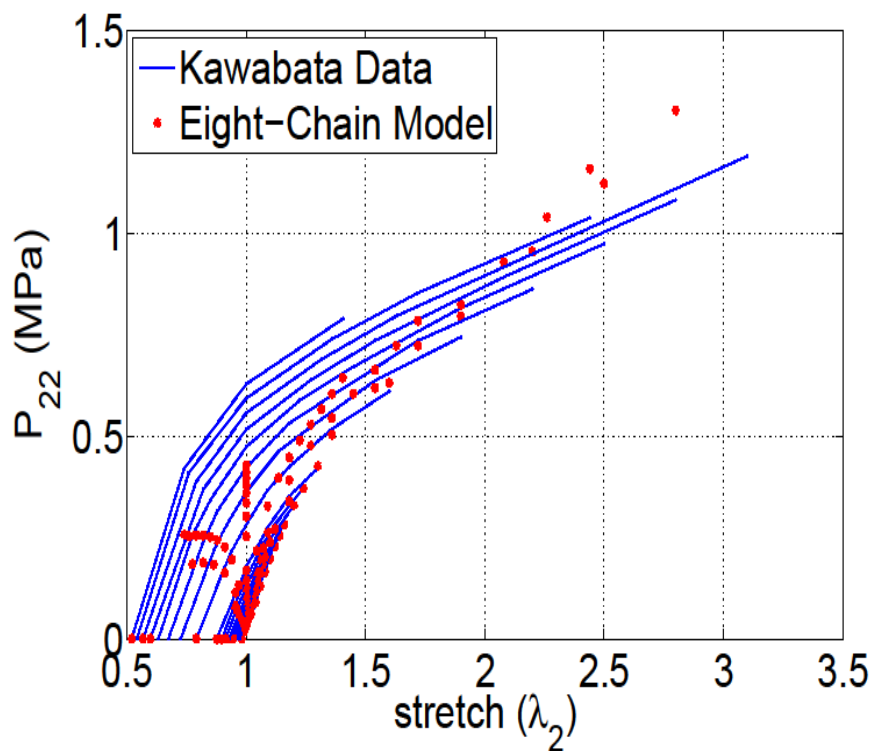
Figure 5.19: Performance of eight-chain model on Kawabata's data for first Piola-Kirchhoff stress $\mathbf{P_{22}}$

5.2.9. Extended Tube Model Results

The performance of extended tube model on Kawabata data is given in Figure 5.20 according to identified parameters in Table 5.3. As it is seen from the plot, extended tube model performance on Kawabata data is remarkable on all deformation regions of λ_2. As it was stated before, extended tube model is the best hyperelastic model among ten hyperelastic models presented in this thesis for biaxial case.
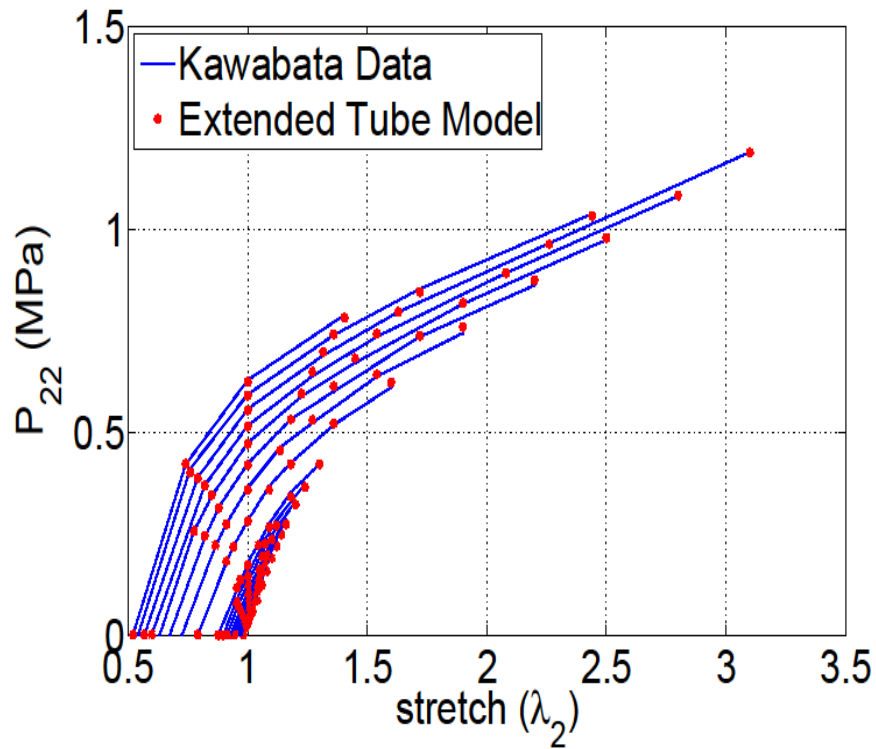
Figure 5.20: Performance of extended tube Model on Kawabata's data for first Piola-Kirchhoff stress P_{22}

5.2.10. Microsphere Model Results

The performance of microsphere model on Kawabata data is given in Figure 5.1 according to identified parameters in Table 5.3. As it is seen from the plot, microsphere model performance on Kawabata data is remarkable on all deformation regions of λ_2.
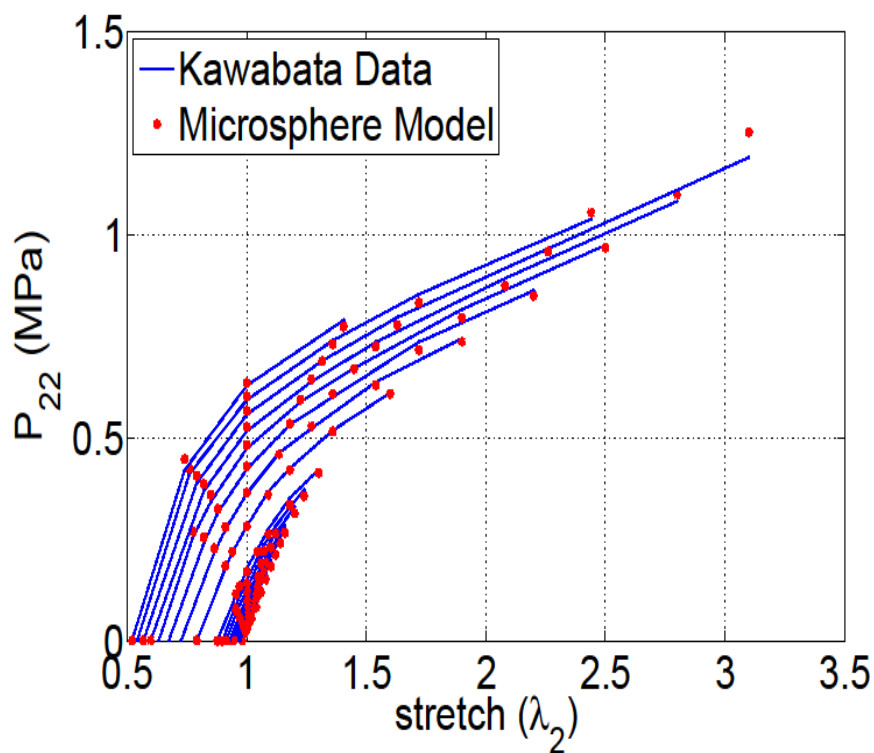

Figure 5.21: Performance of microsphere model on Kawabata's data for first Piola-Kirchhoff stress P_{22}

CHAPTER 6

CONCLUSION

In this study, a multiobjective optimization toolbox for parameter identification of elastomers is developed by using MATLAB GUI to do appropriate elastomer model selection.

In the accessible literature, similar studies to the present study are discussed. It is seen that there are various studies comparing the constitutive hyperelastic models. Several algorithms have been applied to identify the parameters of hyperelastic models in the literature.

In this study, ten constitutive hyperelastic models are compared according to certain criteria. Seven of the models are phenomenological models and three of the models are micro-mechanical models.

Various experiments have been conducted to identify the material parameters of elastomer models. Uniaxial tension, equibiaxial tension, pure shear and biaxial tension experiments are used in this thesis. Treloar data are used for uniaxial tension, equibiaxial tension and pure shear deformation cases whereas Kawabata data are used for biaxial deformation case.

Firstly, continuum mechanics preliminaries are briefed. Strain and stress tensors are introduced here. It is emphasized that elastomers exhibit hyperelastic deformability, so deformed and undeformed configurations must be examined separately unlike small strain theory. The relations between stress tensors are presented in this point. The aim is to have stress-stretch expression of related model for parameter identification process. Isochoric free energy function is used to derive stress-stretch expressions. Isochoric free energy function of each model is introduced in related

73

parts. Then, Kirchhoff stress expression is obtained for each model for desired deformation mode by performing necessary calculations. The first Piola-Kirchhoff stress expression also can be derived after Kirchhoff stress is obtained for each deformation mode of each model. The first Piola-Kirchhoff stress expression is used for parameter identification algorithm.

Afterwards, parameter identification algorithm is presented. MATLAB fmincon is used for parameter identification process. For this MATLAB command, the function to be minimized has to be defined. Least squares method error expression is used to form the function. Summation of uniaxial, equibiaxial and pure shear case error expressions is used for this function. Weight coefficients are also defined for each case to minimize the error because each of the deformation cases may have different errors. Thus, effect of the errors should change on parameter identification process. Since biaxial deformation is evaluated alone, there is only one error expression to be minimized for this case.

After parameter identification process is defined, a multiobjective optimization toolbox development for parameter identification of elastomers is presented. This toolbox is developed in MATLAB GUI. The aim is to perform all the calculations in an easier, faster and more user-friendly environment. This toolbox provides the user to reach the results after making certain selections on the interface.

Ten constitutive hyperelastic models' calculations which were studied in this thesis are coded in this toolbox. Identified parameters, error and necessary plots can be seen in this toolbox so that the user can do the appropriate model selection for specific application. Those identified parameters can be used in finite element calculations.

As it was stated before, Treloar and Kawabata data are used in this thesis for related deformation modes. According to results, Carroll, extended tube, microsphere and Shariff models have the least errors for parameter identification with respect to Treloar data which consist of uniaxial tension, equibiaxial tension and pure shear

cases. However, Carroll model has the advantages of having fewer material parameters and simpler mathematical model compared to other hyperelastic constitutive models for elastomers. But, microsphere model and extended tube models relate macroscopic mechanical behavior to physical structure at molecular level. Yet, one of the other models can be more appropriate for a specific application.

Another material parameter set is identified for each model for Kawabata data. According to results, Shariff, Ogden and extended tube models have the least errors for parameter identification with respect to Kawabata data which consist of biaxial data. Microsphere and Carroll models also show remarkable performances on Kawabata data. However, as it was stated before, extended tube and micro-mechanical models have the advantage of giving a relation between macroscopic mechanical behavior and physical structure at molecular level.

This study presented a multiobjective optimization toolbox development for parameter identification of elastomers. In future works, different parameter identification algorithms can be put forward. Moreover, different toolboxes can be developed for specific applications.

REFERENCES

[1] Vahapoğlu V. Kauçuk Mekaniğinde Yapılan Deneyler. Pamukkale Üniversitesi Mühendislik Bilimleri Dergisi, 19(1):33-60, 2013.

[2] Busfield J. Constitutive Model for Rubbers 3: Proceedings of Third European Conference on Consitutive Models for Rubber. CRC Press, 2003.

[3] Chagnon G., Marckmann G., Verron E. A comparison of the Hart-Smith model with Arruda-Boyce and Gent formulations for rubber elasticity. Rubber Chemistry and Technology, 77:724-735, 2004.

[4] Treloar L.R.G. Stress-strain data for vulcanised rubber under various types of deformation. Transactions of Faraday Society, 40:59-70, 1944.

[5] Kawabata S., Matsuda M., Tei K. and Kawai H. Experimental Survey of the Strain Energy Density Function of Isoprene Rubber Vulcanizate. Macromolecules, 14:154-162, 1981.

[6] Dal H. Approaches to the Modeling of Inelasticity and Failure of Rubberlike Materials: Theory and Numerics. Ph.D. Thesis, Inst. für Statik und Dynamik der Tragwerke, 2012.

[7] Dal H., Kaliske M. A micro-continuum-mechanical material model for failure of rubber-like materials: Application to ageing-induced fracturing. Journal of the Mechanics and Physics of Solids, 57(8):1340-1356, 2009.

[8] Miller K. Testing Elastomers for Hyperelastic Material Models in Finite Element Analysis. Axel Products, Inc.

[9] Vahapoglu V., Karadeniz S. Constitutive Equations for Isotropic Rubber-Like Materials Using Phenomenological Approach: A Bibliography (1930-2003). Rubber Chemistry and Technology, 79(3):489-499, 2006.

[10]   Treloar L.R.G. The Elasticity of a network of long-chain molecules-II. Transactions of Faraday Society, 39:241, 1943.

[11]   Mooney M.J. A Theory of Large Elastic Deformation. Journal of Applied Physics, 11:582, 1940.

[12]   Carroll M.M. A strain energy function for vulcanized rubbers. Journal of Elasticity, 103(2):173-187, 2011.

[13]   Shariff M.H.B.M. Strain energy function for filled and unfilled rubberlike material. Rubber Chemistry and Technology, 73:1-21, 2000.

[14]   Ogden R.W. Large deformation isotropic elasticity-on the correlation of theory and experiment for incompressible rubberlike solids. Proceedings of the Royal Society of London A Mathematical, Physical and Sciences, 326(1567):565-584, 1972.

[15]   Biderman V.L. Calculation of Rubber Parts. Rascheti na Prochnost, 40, 1958.

[16]   Yeoh O.H. Some forms of the strain energy function for rubber. Rubber Chemistry and Technology, 66(5):754-771, 1993.

[17]   Göktepe S. Micro-macro approaches to rubbery and glassy polymers: predictive micromechanically-based models and simulations. Ph.D. Thesis, University of Stuttgart, Germany, 2007.

[18]   Arruda E.M., Boyce M.C. A three-dimensional constitutive model for the large stretch behavior of rubber elastic materials. Journal of the Mechanics and Physics of Solids, 41(2):389-412, 1993.

[19]   Kaliske M., Heinrich G. An extended tube-model for rubber elasticity: statistical-mechanical theory and finite element implementation. Rubber Chemistry and Technology, 72(4):602-632, 1999.

[20]   Steinmann P., Hossain M., Possart G. Hyperelastic models for rubber-like materials: consistent tangent operators and suitability for Treloar's data. Archive of Applied Mechanics, 82(9):1183-1217, 2012.

[21]   Seibert D.J., Schöche N. Direct comparison of some recent rubber elasticity models. Rubber Chemistry and Technology, 73:366-384, 2000.

[22]   Boyce M.C., Arruda E.M. Constitutive Models of Rubber Elasticity: A Review. Rubber Chemistry and Technology, 75:505, 2000.

[23]   Rackle M. Curve Fitting for Ogden, Yeoh and Polynomial Models. ScilabTEC, 7th International Scilab Users Conference, Paris, France, 2015.

[24]   Ali A., Hosseini M., Sahari B.B. A Review of Constitutive Models for Rubber-Like Materials. American Journal of Engineering and Applied Sciences, 3(1):232-239, 2010.

[25]   Wu Y.F., Li A.Q. and Wang H. Parameter identification of hyperelastic and hyper-viscoelastic models. Advances in Structural Engineering and Mechanics (ASEM 15), Incheon, Korea, 2015.

[26]   Nowak Z. Constitutive Modelling and Parameter Identification for Rubber-Like Materials. Polish Academy of Sciences, Institute of Fundamental Technological Research Department of Mechanics of Materials, Warszawa, Poland, 2008.

[27]   Attard M.M., Hunt G.W. Hyperelastic constitutive modeling under finite strain. International Journal Solids and Structures, 41:5327, 2004.

[28]   Cohen A. A Padé approximant to the inverse Langevin function. Rheologica Acta, 30:270-273, 1991.

[29]   Hossain M., Amin A.F.M.S., Kabir M.N. Eight-chain and full network models and their modified versions for rubber hyperelasticity: a comparative study. Journal of the Mechanical Behavior of Materials, 24(1-2), 2015.

[30]   Abu Bakar, M.L.A. Graphical user interface for signal generator. Project paper, Faculty of Electrical & Electronic Engineering, Universiti Malaysia Pahang, 2007.

[31]   Seibert H., Scheffer T., Diebels S. Biaxial Testing of Elastomers – Experimental Setup, Measurement and Experimental Optimisation of Specimen's Shape. Technische Mechanik, 34(2):72-89, 2014.